Development of a Scintillating Reference Grid for Spatial-Phase-Locked Electron-Beam Lithography

by

Mark Alan Finlayson

B.S., University of Michigan (1998)

Submitted to the Department of Electrical Engineering and Computer Science
in partial fulfillment of the requirements for the degree of

Master of Science in Computer Science and Engineering

at the

MASSACHUSETTS INSTITUTE OF TECHNOLOGY

September 2001

Author .....
Department of Electrical Engineering and Computer Science
August 10, 2001

Certified by .....
Henry I. Smith
Keithley Professor of Electrical Engineering
Thesis Supervisor

Accepted by .....
Arthur C. Smith
Chairman, Department Committee on Graduate Students

Development of a Scintillating Reference Grid for Spatial-Phase-Locked Electron-Beam Lithography

by

Mark Alan Finlayson

Submitted to the Department of Electrical Engineering and Computer Science
on August 10, 2001, in partial fulfillment of the
requirements for the degree of
Master of Science in Computer Science and Engineering

Abstract

Spatial-phase-locked electron-beam lithography (SPLEBL) promises significant improvement in the pattern fidelity and placement accuracy of electron-beam lithography by the introduction of feedback into the writing loop. In the planned formulation of SPLEBL, the feedback signal is produced by a reference grid which is bleached into a thin scintillating layer integrated into the electron-beam stack. Formulation and testing of a wide variety of material for use as the scintillating layer are described, in addition to a number of techniques to improve the contrast of the bleached grid. Production of fiducial gratings imaged in a SPLEBL-compatible electron beam system is described, and possible resist stacks that integrate the scintillator for use in SPLEBL are discussed.

Thesis Supervisor: Henry I. Smith
Title: Keithley Professor of Electrical Engineering

Acknowledgments

First, thanks to my advisor Professor Hank Smith. Without him I doubt I would have had the opportunity or desire to come to MIT and conduct graduate studies. He was gracious enough to extend to me an invitation to be a undergraduate researcher in his lab in the summer of 1997, and since then has been extraordinarily generous in his postive regard and support. I am exceptionally grateful to him for the time and energy he has invested in me.

Second, thanks to Professors Roy Clarke, Donald Umstadter, and Duncan Steel at the University of Michigan, and Drs. Ted Bloomstein and Mordy Rothschild at MIT Lincoln Laboratories. These men were my mentors, and I count their encouragement and advice as crucial to my scientific development.

Third, thanks to my many colleages and collaborators at the Nanostructures Lab and MIT at large. Hindy Bronstein for guiding me in the kindest manner possible through my early forays into chemistry. Jim Daley for his clear and kind help, without which most of my efforts would have been futile. Todd Hastings my close SPLEBL collaborator, for continually provided valuable insight and advice, as well as being one of the nicest guys I've ever met. Bernhard Vogeli for many incredibly instructive conversations and insights, as well as a lot of fun. James Goodberlet for being a source of many good ideas and suggestions. Euclid Moon for being indispensible font of information regarding anything computer, car, or electronic music related, and a willing ear for problems large and small. Mike Walsh for being an exceptionally entertaining (not to mention knowledgable and helpful) person. Jimmy Carter for helping out whenever needed. Maithilee Kunda, my RSI mentee, for being instrumental in the final round of data acquisition. Jaime Beers for being a great friend and a constant source of support. The many other members of the NSL for providing a rich, instructive, and fun environment in which to work and be productive: Solomon Assefa, Dave Carter, Maya Farhoud, Dario Gil, Joe Huang, Mike Lim, Mitch Meinhold, Rajesh Menon, Mark Mondol, Tom Murphy, Markus Peuker, Minghao Qi, Tim Savas, Oliver Stoltz, Shingo Uchiyama, and Feng Zhang. My many collaborators at MIT and elsewhere: Tim Long, Professor Tim Swager, Dr. Jason Hafner, Dr. Dave Pflug, and Professor Tayo Akinwande.

Fourth, thanks to my family and my many friends, girlfriends, and acquaintences here in Boston and in the world generally. They are too numerous to mention, but have made my life worth living.

Fifth, thanks to the greco-roman intellectual tradition, as well as western culture and civilization generally, for providing a setting in which neurotic obsession with analytical thinking would give rise to both modern society's love affair with science as well as a place like MIT.

Finally, thanks to all those that I have failed to mention through forgetfulness or willful neglect.

Contents

List of Figures

List of Tables

Chapter 1

Introduction & Motivation

The computer is an extraordinarily powerful calculating tool. The speed and automation of its computations have made possible the solution of problems that previously were too complex for numerical attack. This leverage the computer affords toward the processing of information has been applied across society to astounding effect, and as the device becomes smaller, cheaper, and faster, the scope of its application continuously increases. Indeed, so ubiquitous is the tool presently that its importance cannot overstated.

It is with visions of continuing the astounding increase of the computer's scope and power that an extraordinary amount of time, money, and effort has been expended in improving the speed and reducing the size and cost of the technology. In the forefront of this effort is the thrust to improve the heart of the computer, the microchip. Therein lies the role of this thesis: it describes one facet of a technique which improves a core technology for microchip fabrication, and so finds itself, from an applied point of view, to be a contribution to the effort to increase the computational power which our society has at its disposal.

1.1 Planar Fabrication Techniques for Semiconductor Manufacturing

The general paradigm for the production of microchips was set dramatically in the late 1950's with the advent of planar semiconductor processing techniques. The advantage of the planar process is the speed with which it can produce high quality devices. Original electronic computers (before planar processes) made use of electronic gates called vacuum tubes: small enough to fit in the palm of one's hand, they were painstakingly connected with wires in the complicated ways neccesary to fashion a computing device. The disadvantage with this technique was the amount of space required to house, and the amount of effort to construct the devices. Since computing power scales with the number of gates, early computers filled large rooms. Planar production processes changed all this by making it possible to *integrate*, all at once, thousands of gates (now in the form of transistors) onto the surface of a thin silicon wafer. Before the planar revolution, each macroscopic gate was made individually and hooked together by human hands. After, microscopic gates were produced in parallel, thousands (and now millions) at a time. Thus the birth of the microchip.

The planar method is simple to understand. We will draw a quick analogy to illustrate the principle. Suppose one has an acid which etches away a certain type of ceramic. Also suppose one has a flat dinner plate made out of this very sort of ceramic. If one wished to make a light relief pattern on the surface of this dinner plate (perhaps a pattern that would increase the aesthetic value of the plate), one might proceed as follows: take some wax resistant to the acid, and coat the plate with it. Using a stick or other appropriate scraping device, remove the wax in the desired pattern. Now dip the plate in the acid, wash off the wax, and voila, the relief pattern is etched into the plate. Obviously the technique could be quite sophisticated, employing different sorts of materials, acids, and waxes, different methods for imprinting the wax with the pattern depending on the geometry of the piece, different etching depths depending on how long you left the piece in the acid bath, etc. , etc. This artistic technique is called *lithography*.

Semiconductor lithography works much the same way. In this case the wax is replaced by a material called a *photoresist* (or just *resist*), which is generally a photosensitive polymer The dinner plate is replaced by a

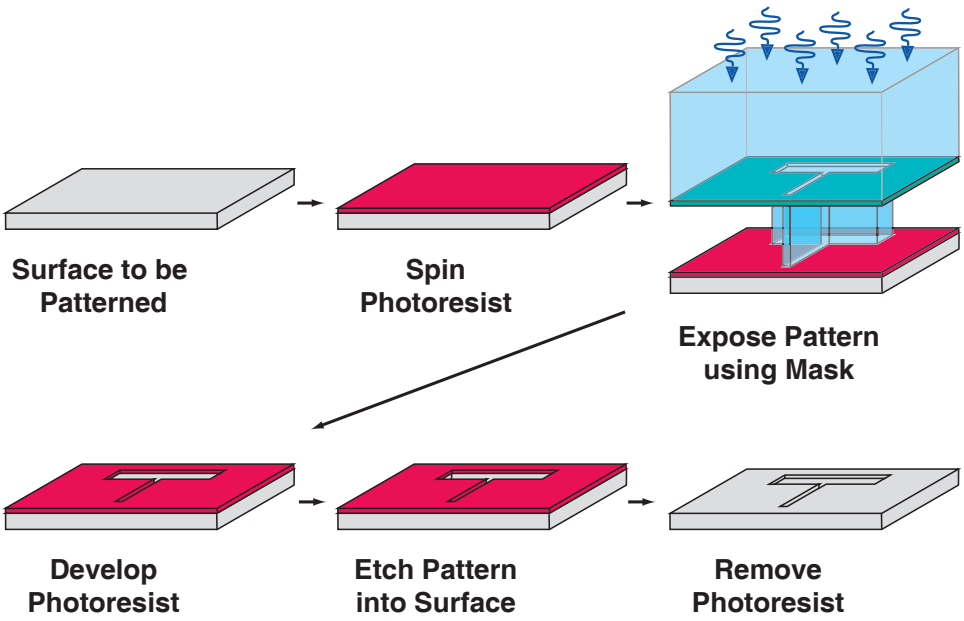

Figure 1-1: The basic lithographic process

silicon wafer. The method for inscribing the pattern in the photoresist consists of projecting light through an optical mask (a stencil of the desired pattern), which then changes the chemical properites of the light-sensitive photoresist in such a way that the pattern can be *developed* in a solvent, much as a photographs are developed after exposure. Once the pattern has been developed in the photoresist, one proceeds with the acid dip and resist removal as usual. The pattern then has been transferred to the silicon. This process is illustrated by rough sketch in Figure 1-1.

The particular transfer process described is termed a *subtractive* lithographic transfer process because it removes material from the surface of interest. Moreover, it is a *wet* process, because the etchant is a liquid. There are *dry* subtractive process which make use of, for example, a plasma to etch or sputter away the material of interest. There are also *additive* processes which add a layer of material to the surface of interest, both those that do and do not involve transferring a pattern. Coupled with a few other more specialized processing techniques (such as ion implantation), one has all the tools with which to make a transistor. An example process to make a metal-oxide-semiconductor field-effect transistor (MOSFET) is illustrated in Figure 1-2.

Not only useful for making microchips, semiconductor processing techniques are applicable to the production of a wide range of interesting devices. Recent attention has focused on microelectromechanical systems (MEMS), integrated optoelectronics, and integrated optical waveguides and filters. These technologies are found everywhere from presentation projectors to automobile airbag inflation sensors to fiberoptic telephone networks.

Once one has the ability to miniturize the transistor, one might ask: by how much do we miniturize it? The answer is "by as much as possible" [38]. The smaller a transistor is, the faster they are able to switch, improving performance, and the more of them fit on a single wafer, lowering cost.

Currently the size of transistors is limited by the resolution of optical lithography. This resolution is set by the diffraction limit of light, in that features smaller than half the wavelength cannot be printed due to blurring caused by diffraction of the pattern. Consequently, to print smaller transistors industry is constantly moving toward shorter and shorter wavelengths. Eventually, it is likely that they will implement a mask-based next generation lithography (NGL) such as x-ray or deep-ultraviolet wavelengths, which will hand off the size limitations to other factors [2].

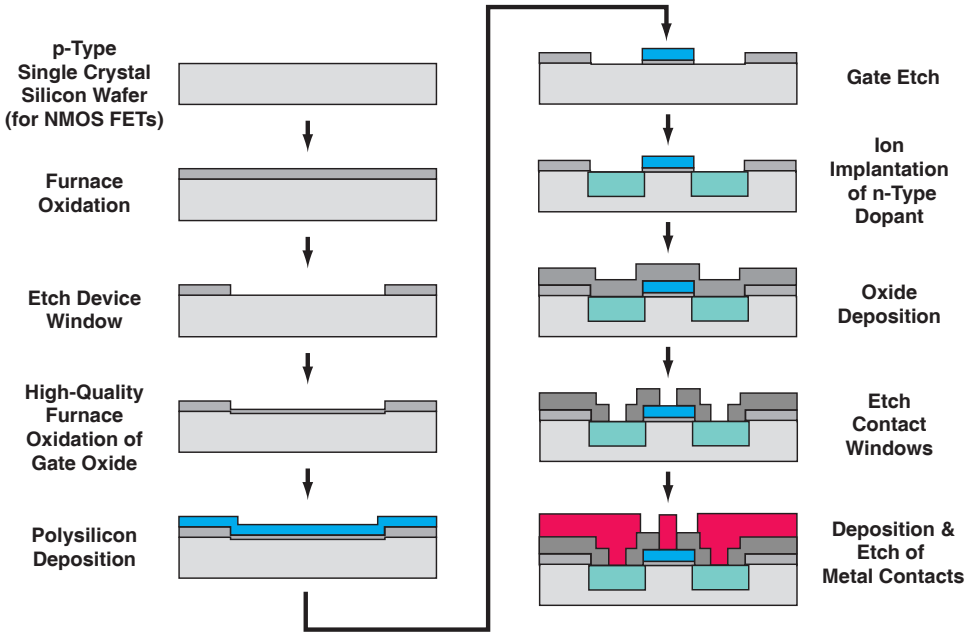

Figure 1-2: A basic MOSFET process

1.2 Electron-beam Lithography

One major hurdle in a mask-based next generation lithographic process would be the production of an error-free mask. Small feature sizes are irrelevant if feature placement is not well controlled – in other words, it hardly matters if you can print 30 nanometer features if you can't put them where you want them to be within 30 nanometers. Indeed, for any particular critical feature size one wants to print, some small fraction of that size is usually required in placement accuracy to ensure proper device performance. Future requirements considered as a bare minimum for pattern placement are shown in the Semiconductor Industry Association roadmap (Figure 1-3).

The current technique of choice for making lithographic masks is electron-beam lithography (EBL). Its operation is illustrated in Figure 1-4. It is similar to optical lithography in that it uses a resist and deposits energy into that resist to change its development properties. For electron-beam lithography, however, the

Year / *Technology Node*	*2008* *70nm*		*2011* *50nm*	*2014* *35nm*
Lithography technology	Optical	NGL	NGL	NGL
Image placement (nm, multi-point)	15	15	12	9
CD uniformity (nm, 3 sigma)				
Isolated lines (MPU gates)	10*	7	5	3
Dense lines (DRAM half pitch)	14*	11	8	5.6
Contact/vias	8	12	9	6.4
Linearity (nm)	10		7	5
CD mean to target (nm)	6		5	4

Solutions Being Pursued *No Known Solutions*

Figure 1-3: Semiconductor Industry Association Roadmap, Mask Requirements, 1999 [1]

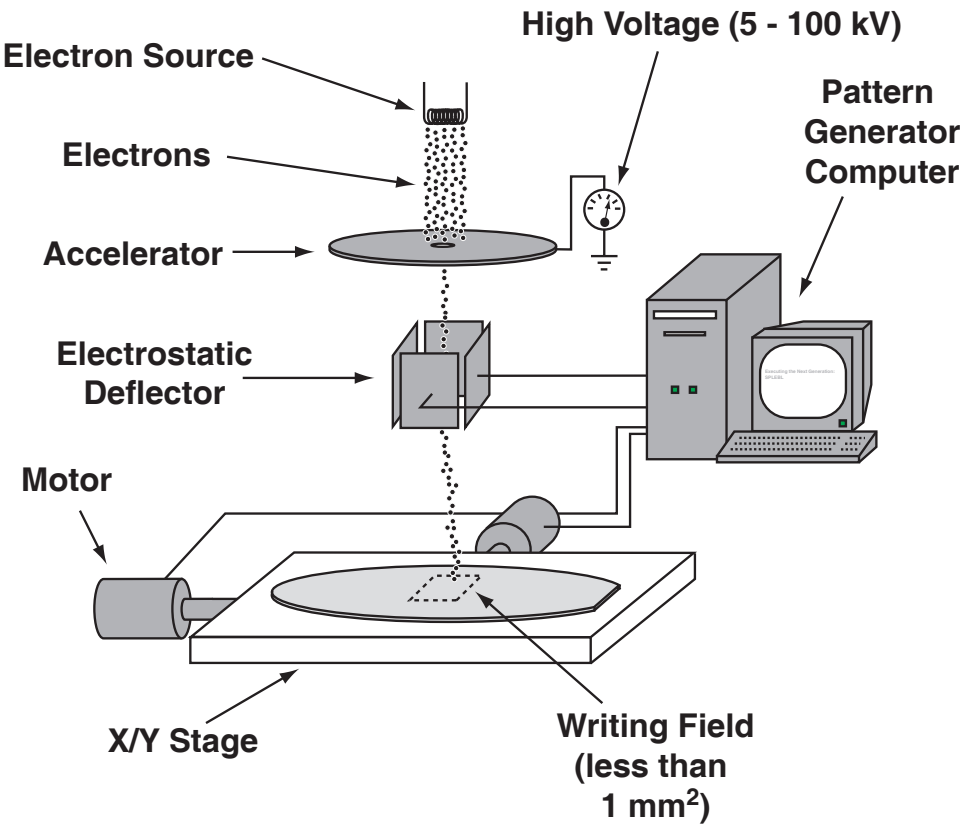

Figure 1-4: Electron-beam lithography

method of energy deposition is a computer-controlled electron beam, which writes features in a serial, rather than parallel, manner. Due to the nature of electron-beam optics the machine has only a small field of view, so a mechanical stage is usually required to move the substrate about (in a stop-and-go or continuous fashion) so as to access all areas on which patterns are to be written. After writing, the lithography is conducted normally, i.e., by development and pattern transfer.

Electron-beam lithography suffers from problems such as stage drift and electrical interference, inherent to its design. These can be problematic, as they affect the beam position on the sample after the computer calibration. Due to these inherent limitations, electron-beam lithography's capabilities for pattern placement will be outstripped by the roadmap requirements by 2008.

1.3 Spatial-phase-locked Electron-beam Lithography

Spatial-phase-locked electron-beam lithography (SPLEBL) is today the only technique which promises to overcome these limitations [36]. In its essence, the technique introduces feedback into the writing loop, as shown in Figure 1-5), via the detection of the interaction between the electron beam and a reference grid

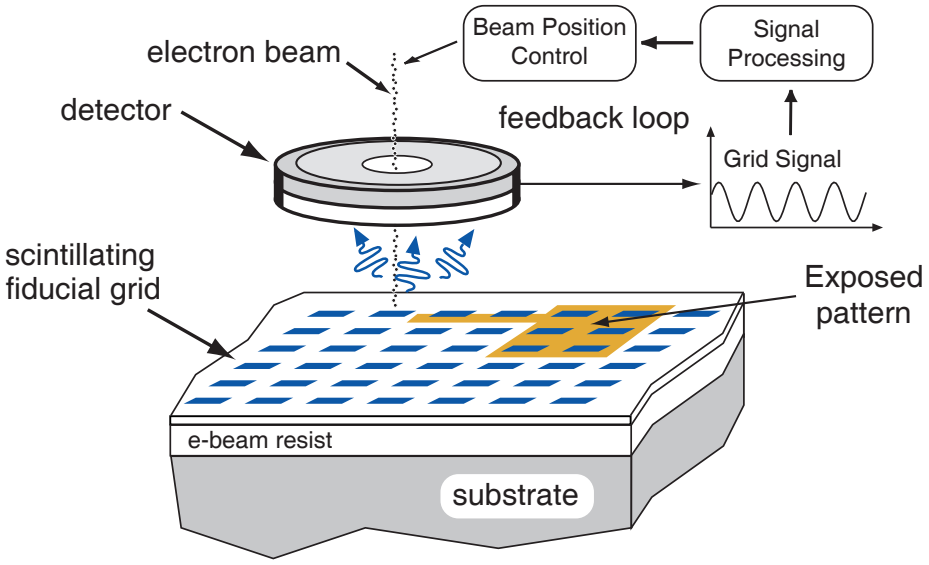

Figure 1-5: Spatial-phase-locked electron-beam lithography

incorporated into the resist stack. As the electron-beam scans the wafer in the course of writing a pattern, the grid-beam interaction produces a periodic signal which is returned to the EBL computer. This allows for patterns to be directly registered to the grid in real-time. Ideally, production of such a highly accurate grid (the *fiducial grid*) is achieved via interferometric lithography (IL) [32]. With SPLEBL, it is predicted that a pattern placement accuracy of less than one nanometer is achievable [15].

Key to the SPLEBL effort is the physical implementation of the fiducial grid. Several constraints govern the choice of a materials system and patterning process: First and foremost, the grid should be easily patterned, directly or indirectly, with interference lithography. This allows reference to the accurate standard of the wavelength of light. Second, electron-beam writing should proceed unmolested, and so the grid-beam interaction should not interfere with beam resolution or placement. Third, the grid signal must have a good signal-to-noise ratio and allow for fast transduction so as not to slow writing. Fourth, the grid must be compatible with subsequent processing (i.e., pattern transfer). Fifth and finally, as in any modification of an already successful technique, a minimum of complexity is desirable.

1.4 The Scintillating Fiducial Grid

It is likely there are many solutions which satisfy these grid design constraints. We will concern ourselves with a single one, detailed as follows.

The idea is based upon *scintillation* coutning, which employs ogranic molecules which quickly and efficiently emit light (usually in the visible) upon the absorption of high-energy radiations. The phenomenon is not the one familiar from everyday life in the form of glow-in-the-dark toys or faintly luminescent signs. That is called *phosphorescence*, which is the emission of light from a substance with a characteristic time that is generally very slow (many milliseconds at least, if not seconds). Rather, *fluorescence*, or *scintillation*, is the prompt emission (tens of nanoseconds at its fastest) of visible radiation directly following excitation [24, Chap. 8]. This latter phenomenon is the detection method in which we are interested.

In addition to being scintillators, many of these molecules degrade under ultraviolet illumination in the presence of oxygen, meaning they are susceptible to patterning with interference lithography. By spinning a solution of plastic and flourophores in the same way resist is spun, the scintillating molecules can be held near the surface of the substrate in a plastic thin film. Proper choice of the flourophores and plastic can insure a bright and robust signal with a good bleaching characteristic, while the low density of the layer

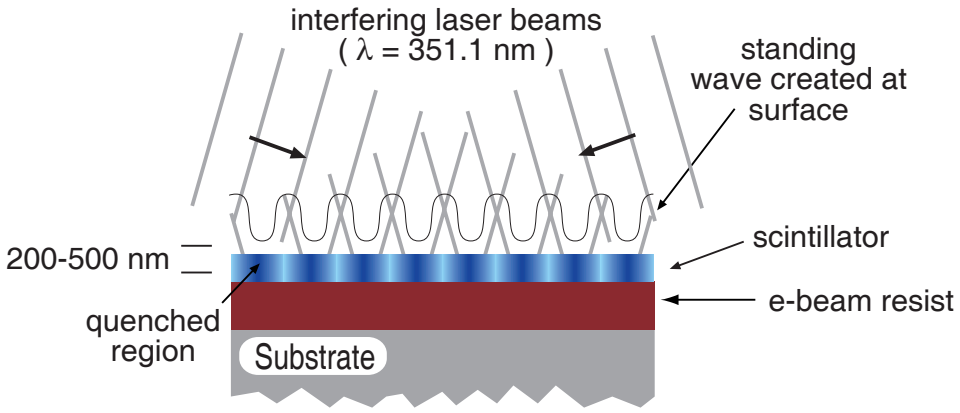

Figure 1-6: Interference lithography used to bleach the fiducial grid

promises minimal interference with electron-beam lithography. Thus it can be seen that the scintillating fiducial grid satisfies, at least at first glance, the first three requirements for the fiducial grid.

In regards to having the thin plastic scintillating layer (from now on, a *scintillator*) satisfy the forth requirement, there is potentially quite a bit of trouble in store. Ideally, it would be desired that the scintillator could be spun on and washed off without affecting resist, no matter what the resist might be. In other words, no property of the scintillator would be tied to any property of the resist, so that allowing SPLEBL to be portable across a range of electron-beam lithography setups. In reality this may be difficult to achieve, and certainly was not achieved under the auspices of this thesis. As will be covered in the next chapter, many of the common electron-beam resists dissolve in the same solvents that dissolve the scintillator, so in the absence of the identification of an appropriate solvent, the stack may require an interlayer. Moreover, the wavelengths of light used to achieve good bleaching contrast with the scintillators also expose certain electron-beam resists, requiring a scintillator-on-bottom and grid-exposure-first scheme, with an interlayer. With this sort of scheme, some sort of trilayer pattern-transfer technique would be required, thus clearly putting in danger satisfaction of the fifth requirement, that of simplicity. These issues will be discussed in more detail later in Section 2.7.

Before work on this thesis was begun, one formulation of a scintillator had already been tested [18]. This thesis will describe the search for scintillators that are brighter and have higher contrasts, and thereby make SPLEBL a feasible technique. More generally though, this thesis describes the development of an essential component of the SPLEBL technique, and so finds itself as a contribution to the improvement of electron-beam written patterns, and thus can be thought of improving our ability to produce, via semiconductor lithography, large planar patterns of extraordinarily high resolution and fidelity, an ability which is interesting for its application to a wide variety of important technologies.

Chapter 2

Overview of Scintillators

This chapter gives an overview of the theoretical underpinnings of the experimental work in this thesis. A familiarity with quantum mechanics at the graduate level and chemistry at the undergraduate level is assumed. The first three sections review the quantum mechanics of organic molecules and energy transitions, which gives an indication of the complicated connections between molecular structure and the observed properties of molecules, as well as allow us to understand how the molecules absorb energy from the incident electrons and transform it into light that is used in the SPLEBL feedback signal. Section 2.4 discusses briefly the photochemistry of the bleaching of organic scintillators. Finally, solvents and their attendant properties, which are of key importance to laying down and removing the thin polymer layer in which the grid is bleached, are reviewed in the last three sections.

2.1 Quantum Mechanics of Scintillating Organic Molecules

Excellent references for the material in this section, drawn upon heavily here, are I.N. Levine, *Quantum Chemistry* [26], P.W. Atkins, *Molecular Quantum Mechanics* [3], and N.J. Turro, *Modern Molecular Photochemistry* [40].

Some organic molecules emit light and others do not. Why is this? What properties of molecules correlate with their fluorescence, and so might have an effect on the engineering of a plastic scintillating grid? Insights into the answers to these questions will be found in a quantum mechanical sketch of scintillating molecules.

Given some skeletal nuclear framework for a molecule, one possible starting point for any quantum mechanical analysis of that molecule would be the Schrödinger Equation:

$$\hat{H}\psi(\bar{x}) = E\psi(\bar{x}) \tag{2.1}$$

which describes the wavefunction, $\psi(\bar{x})$, of that system. Theoretically an accurate wavefunction is a complete description of the system, and any information about that system it is possible to know can be had with the proper manipulations.

Key to an accurate wavefunction is an accurate Hamiltonian. A molecular Hamiltonian might be as follows:

$$\hat{H}_{mol} = -\frac{\hbar^2}{2}\sum_{\alpha}\frac{1}{m_\alpha}\nabla_\alpha^2 - \frac{\hbar^2}{2m_e}\sum_i \nabla_i^2 + \sum_\alpha\sum_{\beta>\alpha}\frac{Z_\alpha Z_\beta e^2}{r_{\alpha\beta}} - \sum_\alpha\sum_i\frac{Z_\alpha e^2}{r_{i\alpha}} + \sum_j\sum_{i>j}\frac{e^2}{r_{ij}} \tag{2.2}$$

where the first term describes the electronic kinetic energy, the second the nuclear kinetic energy, and the last three terms describe the various electrostatic forces, namely, the nuclei-nuclei, nuclei-electron, and electron-electron forces, respectively. This description is somewhat simlpistic in that it assumes the nuclei and electrons are point masses, and neglects spin-orbit and other relativitistic interactions. Again, some starting nuclear framework of a particular molecule under investigation is assumed.

As one might imagine, solving the Schrödinger equation with this Hamiltonian would be quite onerous, and probably would yield results so inaccurate or convoluted as to be useless. A number of simplifying

approximations can be applied to the equation to facilitate the construction of more insightful wavefunctions. These will include: 1) an approximation to separate nuclear and electronic portions of the wavefunction, and 2) an approximation to simplify the thus derived electronic portion of the wavefunction.

The approximation to separate the nuclear and electronic portions of the wavefunction is called the Born-Oppenheimer approximation, where the fact that nuclear masses are much larger than the electronic mass allows the molecular Hamiltonian to be written as a sum of nuclear and electronic Hamiltonians:

$$\hat{H}_{el}\psi_{el}(q_i;q_\alpha) = E_{el}\psi_{el}(q_i;q_\alpha) \tag{2.3}$$

$$\hat{H}_{nuc}\psi_{nuc}(q_\alpha) = E_{nuc}\psi_{nuc}(q_\alpha) \tag{2.4}$$

To obtain a full solution to the equation, and thereby describe the molecule as accurately as allowed by the approximation, the electronic portion of the Born-Oppenheimer approximation to the Shrödinger equation, Equation 2.3, is solved for each set of nuclear coordinates, q_α. The electronic energy, then being a function of the nuclear coordinates, serves as an effective potential, $\mathcal{U}(q_\alpha)$, in the nuclear part of the Born-Oppenheimer approximation, Equation 2.4, allowing solutions for the wavefunctions of the nuclear masses and an understanding of their small departures from equilibrium.

The approximation is applied to the electronic portion of the wavefunction, $\psi_{el}(q_i;q_\alpha)$, is the Molecular Orbital approximation. This approach gives insight into the extended spatial shape of the molecular orbitals, and why conjugation of double bonds is important to the properties of scintillating molecules.

The molecular orbital approximation builds electronic wavefunctions from atomic wavefunctions (the basis set) by adding them linearly to one another, with weighting coefficients determined by variational methods that minimize the energy. This method is also called the *Linear Combination of Atomic Orbitals* method, or LCAO method. The atomic wavefunctions in the basis set are generally drawn from the s- and p-orbitals in the valence shells of all atoms in the molecule, with symmetry conditions dictating which linear combinations are appropriate. Depending on whether these LCAO orbitals, or *hybrid* orbitals, change sign under a spatial inversion, they are called antibonding or bonding orbitals.

In the case of a diatomic homonuclear molecule the types of molecular orbitals (bonds) naturally fall into two classes, called σ and π. Those orbitals that contain combinations of s- and p_z-orbitals, and that have rotational symmetry about the internuclear axis, are σ-bonds. Those that are combinations of p_x- and p_y-orbitals, and are not rotationally symmetric about the internuclear axis, are π-orbitals. The benefits of this classification are numerous: σ-bonds are generally the core bonding orbitals, being held close to the internuclear axis, and form, in a sense, the 'skeletal' structure of the molecule, whereas π-orbitals are on average further away from the nuclei and so are higher in energy (more weakly bound) and are thus more susceptible to chemical attack. The angular orientations of the bonds is found in the same manner as were coefficients of the hybrid orbitals themselves, that is, by a variational calculation which minimizes the energy. Through this sort of calculation it is found that for minimum orbital energy (which results from a maximization of the orbital overlap integral) the σ-bonds impose no restriction on rotation about the internuclear axis, while π-bonds restrict its constituent p-orbitals to the same orientation. In other words, a p-orbital on one atom contributing to a particular π-bond must point in the same direction as the p-orbital on its bonding partner which is associated in the same bond, and so a π-bond is torsionally rigid.

For polyatomic molecules with more complex geometries, the s and p contributions to each molecular orbital become more complicated, but we can still benefit from a rough σ and π classification. Any particular σ-bond will still be roughly symmetric about whatever internuclear axis it is associated with, and will contain a large amount of s-orbital character, while a π-bond will generally be found much further out from the same internuclear axis, and will have mostly p-orbital character. Once these polyatomic π-orbitals are recognized as such, it is easily recognized that they have the same sort of torsional rigidity as do their diatomic counterparts. The molecular orbital technique shows, moreover, that under certain symmetry conditions, these π-orbitals can be *conjugated*, where p-orbitals on a set of neighboring atoms can join together to form one large distributed *π-system*. It is these π-systems which give rise to the the most salient features of scintillating molecules, and which will most affect our engineering of a scintillating grid.

A π-system can be considered as merely one large orbital, the same as any other, except it is widely distributed across many atoms. Many important properties of these π-systems can be understood by analogy

with the particle-in-a-box problem from rudimentary quantum mechanics. In this conceptualization, the portion of the nuclear skeleton across which the π-system is distributed can be thought of as the confining well, and the electrons the particles in that well. Since the size of the well increases (i.e., as one moves to molecules with more conjugation) the energy of those levels (orbitals) decrease, and the spectrum shifts to the red. As the size of the molecule limits the possible number of conjugated bonds, we will find that the converse is also true for the most part: the smaller the molecule, the more toward the blue one will find its spectrum.

In addition to their spectroscopic properties, π-systems also lend torsional rigidity to the bonds they cover (relative rigidity, at least, in the face of normal thermal and collisional stresses encountered in the everyday life of the molecule). This rigidity, in the case of three or more atoms connected together in the system, gives rise to a planarity of that portion of the molecule. In the case of conjugated ring systems (so called *aromatic* systems), where a π-orbital extends across a set of atoms connected head-to-tail, this rigidity can be especially robust.

Now that we have sketched a basic quantum mechanical picture of the orbitals of molecules, which are the font from which the emissive properties of molecules flow, we can ask the following question: Are all molecules containing π-systems equally good scintillators? The answer is, of course, 'No'. Some conjugated molecules emit very strongly and quickly when excited, others emit slowly, and still others emit not at all, or at best imperceptibly. Whence the difference? Simply, it arises out of the different transition rates between orbitals, which are governed by Fermi's Golden Rule:

$$rate = \frac{2\pi}{h}\rho|\langle\psi_i \mid \hat{O}_c \mid \psi_f\rangle|^2 \tag{2.5}$$

where ρ is the density of final states capable of coupling with the intial state, and $\hat{O}_c$ is the operator corresponding to the perturbation that couples the initial and final states. It is important to note that this rule is a first order perturbation calculation, and thus an approximation. We are concerned with five types of transitions in the scintillating molecules, each with a different form of operator and involving either the nuclear and electronic wavefunctions (or both): radiative absorption, radiative emission, nonradiative relaxation, vibrational relaxation, and intersystem crossing. Radiative processes involve a change of state from one electronic orbital to another, along with a change of parity. Emission or absorption of a photon accounts for a majority of the difference in momentum and energy. Nonradiative relaxation involves the conversion of electronic energy of a higher electronic state into nuclear vibrational energy of a lower electronic state. Vibrational relaxation involves a relaxation to lower nuclear vibrational sublevels inside of a single electronic state, sometimes through collisions with other molecules, other times radiatively. We do not include these under radiative transitions though, as the photons are of too low an energy to be of interest to us with regards to scintillation phenomenon. Finally, intersystem crossing involves a transition between states with a spin flip, either with or without the subsequent emission of a photon.

Now we can begin to see how a molecule might contrive to be a scintillator, or not, depending on its transition rates. If the primary excited state (perhaps a singlet) couples strongly (perhaps through a nonradiative intersystem crossing) to a triplet state, and that triplet state is metastable because its primary means of deexcitation is through a very slow radiative intersystem crossing to the ground state (a singlet), the molecule will be a phosphor: that is, it will radiate, but only very slowly. If the excited state is strongly coupled to the ground state through a nonradiative transition, then the molecule will not scintillate at all. Moreover, if the method of initial excitation of the molecule is not absorption of a photon, but rather is a collision with a ionizing particle (such as a high-energy electron), there may be more than one initial excited state, perhaps with wildly different energies, and perhaps also of both singlet and triplet character. This further complicates the problem, and can lead to a scintillator that is inefficient under photon excitation but much more efficient under electron excitation, or vice versa. With all these factors in mind, we might conclude that it is rare when the excited state of interest couples strongly in a radiative fashion to a state which is far removed from it in energy, thus making rare a good scintillator which is both bright and fast.

Now that we have sketched a picture of organic scintillators and how they work, it is easy to see that scintillation is a complex phenomenon. Even with an identity coupling operator in Equation 2.5, we can see that the rates will depend in a complicated manner on the wavefunctions of the states, which themselves depend in a very complicated manner on molecular geometry and composition. A full treatment of the

problem, with the coupling operator and perhaps fuller perturbative expansion, makes predicting transition rates *a priori* a daunting task. Add to this the fact that other properties of the molecule important to our purposes (such as reactivity, stability, and solubility) also devolve from the quantum mechanics of the molecule, it becomes clear that rational design of organic scintillators is an extraordinarily difficult task, and the general approach for identifying molecules appropriate for one's purposes is to resort to catalogic investigation, as we do later in this work.

2.2 Electron Interactions with Polymer films

With the above background on the mechanics of the individual scintillators now clear to us, we turn our attention to the method for producing excited states in the first place.

As indicated earlier, our method for probing the scintillating plastic is a narrowly focused electron beam at kilovolt energies (2 to 100 kV). Quite a bit of theoretical work has been done concerning the interaction of high-energy electrons with matter. Most important for our purposes is Bethe's equation [24, Chap. 2], which describes *collisional* losses for electrons in a solid.

$$-\left(\frac{dE}{dx}\right)_c = \frac{2\pi e^4 NZ}{m_0 v^2}\left(ln\frac{m_0 v^2 E}{2I^2(1-\beta^2)} - (ln2)(2\sqrt{1-\beta^2} - 1 + \beta^2) + (1-\beta^2) + \frac{1}{8}\left(1-\sqrt{1-\beta^2}\right)^2\right) \tag{2.6}$$

where v and e are the velocity and charge of the incident electron, N and Z are the number density and atomic number of the absorber atoms, I is the ionization potential of the absorber, $\beta \equiv v/c$, m_0 is the electron rest mass. Solution of this equation for a zero-crossing in the energy gives a characteristic path length of the electron in the solid, called the *Bethe range*. Linear specific energy loss through bremsstrahlung, or *radiative*, processes are described by another of Bethe's equations [24, Chap. 2]

$$-\left(\frac{dE}{dx}\right)_r = \frac{NEZ(Z+1)e^4}{137 m_0^2 c^4}\left(4\ln\frac{2E}{m_0 c^2} - \frac{4}{3}\right) \tag{2.7}$$

The ratio of the radiative to the collisional energy loss terms is given approximately by

$$\frac{(dE/dx)_r}{(dE/dx)_c} \approx \frac{EZ}{700} \tag{2.8}$$

where E is in units of MeV. Thus for a carbonaceous polymer, where Z is the range of 10, with a 100 keV incident electron, the collisional energy loss term is approximately 700 times the magnitude of the radiative loss term, and so the latter can safely be ignored. The amount of energy deposition per unit path length, then, looks like as shown in Figure 2-1, with most of the electron energy being deposited at the end of its path.

Important to consider as well is that the incident electrons are equal in mass to the orbital electrons, allowing them to lose a large amount of energy in a single collision and create excited or ionized states in the material containing the orbital electrons. Furthermore, the electron mass is much less than that of any nucleus, so an electron-nucleus collision can result in a large-angle scattering event. Due to these two factors, electrons suffer a great deal of scattering as they pass through an absorber, and their penetration depth (measured along the normal to the surface) is often much less than the length of their path inside the absorber.

Monte Carlo simulations taking elastic and inelastic collisions into account can give a good prediction of energy deposition in the solid as dependent upon position [25]. These simulations have shown that there is a significant energy spread in the beam as it passes through the solid. This spread narrows with increasing beam energy, while the electron path length increases with increasing beam energy. Both of these are attributable to the fact that the electrons scatter less at higher energies. These facts have implications for the excitation width inside of polymers, which will be dealt with in Chapter 3.

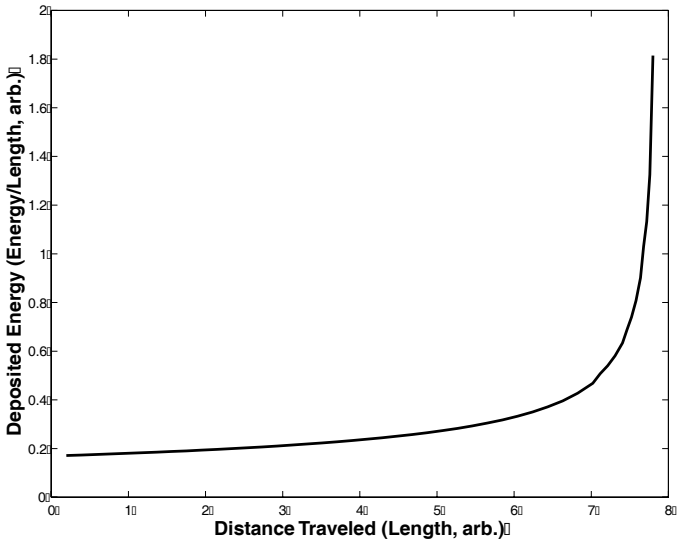

Figure 2-1: Electron energy deposition per unit length versus path length inside a solid material

2.3 Energy Transfer in Plastic Scintilators

Finally, to have a full picture of the emissive properties of plastic scintillators we will be using, it is important to understand, via the quantum mechanics, the mechanisms of energy transfer from one component to another inside of the plastic.

Energy absorption from incident electrons causes transistions to excited molecular orbital states in both polymers and fluorophores. The main mechanism of energy transfer in this case is inelastic collisions, which are relatively indiscriminate in which molecules they excite. Because of this, the amount of energy deposited in each component roughly corresponds to the relative densities of each component weighted by their weight percent in the mixture. Since the polymer forms the bulk of the mixture, most of the energy is deposited there.

Once an excited state exists, the energy can migrate from molecule to molecule (or from functional group to functional group, in an intramolecular fashion) via one of several energy transfer mechanisms, including radiative, coloumbic, or electron exchange transfer mechanisms. These energy transfers are critical to the operation of the scintillator. They allow the energy absorbed in the polymer to be transfered quickly to an efficient scintillator, and from there waveshifted by an efficient absorber/reemitter molecule.

The radiative mechanism is the simplest, involving merely the uncoordinated exchange of a photon emitted from the donor to the acceptor molecule. This transfer depends on a number of factors, including the efficiency of emission by the donor, the efficiency of absorption by the acceptor, the concentration of the acceptor, and the spectral overlap integral between the two molecules, which measures the amount of overlap there is between the emission and absorption spectrums of the donor and acceptor, respectively.

The coloumbic mechanism of energy transfer involves a dipole induction on the acceptor molecule by the donor molecule. This can be treated quantum mechanically in the same way as normal, intramolecular transistions, by the use of Fermi's Golden Rule (cf. eq. 2.5). Förster derived an expression for the rate of this energy transfer by relating it to the interaction energy of two dipoles with transition dipole moments μ_D and μ_A [40]:

$$k_{ET}(dipole) \sim J\frac{\mu_D \mu_A}{R_{DA}^6} \tag{2.9}$$

where J is the spectral overlap integral and R_{DA} is the donor-acceptor separation. The transition dipole moments are further related to molecular properties such as the magnitude of the pure radiative rate constant

for the donor and the extinction coefficient for the acceptor (both related to the strength of their associated transitions). As can be seen by the inverse dependence of the sixth power of the separation, this is an extremely short range interaction between the molecules.

Finally, the electron exchange mechanism of energy transfer is a purely quantum mechanical effect, again governed by Fermi's Golden Rule (cf. eq. 2.5), which involves the direct exchange of an electron between the excited states of the donor and acceptor molecules, along with the direct exchange of an electron between two lower states. It can occur in one of several ways, included concerted exchange (where the electrons are exchanged simultaneously), charge transfer (where the electrons of the donor and acceptor exchange in a stepwise manner through a radical ion pair), or bonding exchange (where an intermediate diradical or zwitterion formed by chemical bonding causes the exchange). Dexter derived an expression for the rates of these sorts of transfers [40]:

$$k_{ET}(exchange) \sim J \exp\left(-2R_{DA}/L\right) \tag{2.10}$$

where J is the spectral overlap integral, R_{DA} is the donor-acceptor separation, and L is the van der Waals radii of the molecules. As this mechanism of exchange depends exponentially on inter- or intramoleculear separation, it drops to negligibly small values at distances greater than a few molecular radii.

Now that all the possible forms of energy transfer have been enumerated, we can examine which forms are dominant in the plastic scintillators we will be examining in this work. A typical energy path is shown in Figure 2-2 for a plastic scintillator containing a polymer host, two scintillators, and an additive (naphthalene) (specifics of the varius compositions of scintillators are discussed in Section 4.1). The first point to note is that energy transfer very often takes place along the polymer backbone. This non-radiative transfer allows the scintillator to be much more efficient than it would be normally, as the energy can travel quite a distance to find a scintillator to transfer to and then be emitted as light. This effect is documented experimentally in the increase (to a limit) of scintillation efficiency with molecular weight of the polymer chains [5, §9.3]. Experimental studies have shown that the initial transfer of energy from the polymer to the fluors takes place by non-radiative mechanisms [5, §9.10]. On the other hand, energy that passes through the primary scintillator is transferred primarily by radiative mechanisms to the secondary scintillator.

2.4 Photochemistry of Organic Fluors

Convenient to the production of a viable scintillating fiducial grid is the ability to bleach the scintillation using interference lithography. *Bleaching* is defined as the effect that, upon exposure to light of some wavelength, the scintillating film undergoes a change in character that permanently reduces (bleaches) the light ouput. How much bleaching is required will be determined by the signal processing constraints of the SPLEBL implementation [22], but will in all likelihood be as much as possible. This means that the scintillator should have a high *contrast*, a high ratio between the scintillation intensity in the unbleached versus the bleached regions.

In the general case the polymer hosts and scintillators are susceptible to any number of photodriven chemical reactions that might serve to break down the structure of the molecules and render them nonfunctional, thus breaking the energy transfer chain. For example, it is well known that PMMA will undergo chain scission at wavelengths in the deep ultraviolet, which will reduce the average polymer molecular weight dramatically and thus the scintillation efficiency [28]. As another example, anthracene is susceptible to oxidation at its 9 and 10 positions, making the formation of the non-emissive anthraquinone a distinct possibility [40].

Indeed, molecules generally can be extremely reactive under photonic stimulation, since their excited states are high in energy and wholly unstable. Unfortunately, the possible photoreactions are legion, including additions, substitutions, isomerizations, rearrangments, or fragmentations [40]. Moreover, the composition of the scintillators, with a host polymer and up to three different complex molecules, complicates matters further. All of this makes it difficult to predict reaction pathways, and we must rely on experiment to demonstrate which molecules bleach effectively under what conditions.

That said, there are a few general points one can garner from the experimental evidence. First, the presence of oxygen is usually critical to the dominant bleaching reactions. This has been shown several times in the literature [5], as well as in this thesis. In the experiments conducted in the NSL, the thin

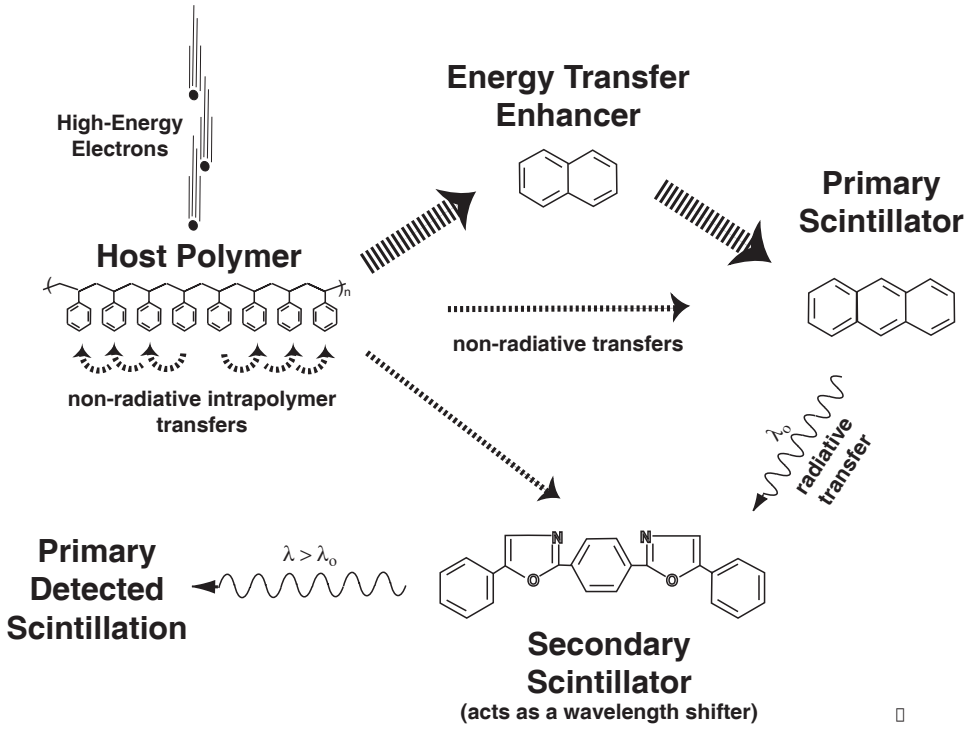

Figure 2-2: General energy pathway in a typical multi-component plastic scintillator

scintillating film was covered with a thin oxygen-impermeable layer of silicon dioxide, deposited by electron beam evaporation. The deposition was conducted under low vacuum (microtorr) and was about 30 nm thick. This layer, while allowing light through, effectively stopped any bleaching from taking place.

Second, the degree of bleaching is highly dependent on the wavelength of light used. As will be seen later in this work, bleaching with 351 nm wavelength light is clearly not as effective as 220 nm wavelength light. This was somewhat expected, as the higher wavelength light probably excites higher, more reactive states, in addition to forming full-fledged, highly reactive ions.

Finally, it is important to note that the electron beam stimulation will in the general case drive at least the same, if not more, reactions as are driven by optical stimulation. This could be a major problem, as during a SPLEBL write scattered electrons might bleach the scintillation in further up along the beam path, thus reducing the effective contrast of the bleaching. This problem can be dealt with by choosing more robust scintillators, but it is not yet clear if this will be limiting factor in SPLEBL; it is an issue that must be addressed [22].

2.5 Solvation and Solvent Systems

A key issue for the development of a scintillator is that of the casting and dissolution solvents. Because the resist in the stack is also a polymer film, and is susceptible to dissolution and damage by solvents, it is critical that one chooses the a solvent that effects only the scintillator and not the resist.

Several characteristics of a solvent and a solute determine whether or not they will form a solution. The first of these is their relative cohesive energy densities. The cohesive energy density, δ, is related to the heat of vaporization (here denoted as c) as indicated in the expression:

$$\delta = \sqrt{c} = \left[\frac{\Delta H - RT}{V_m}\right]^{1/2} \tag{2.11}$$

where ΔH is the heat of vaporization, and V_m is the molar volume. The heat of vaporization is the amount of energy required to separate all the molecules of an aggregate state (a liquid or solid) to a widely distributed gaseous state. In other words, the heat of vaporization measures how much energy is bound up in the interactions between the molecules. Solvents and solutes with similar types of cohesive energy density will be able to intermix easily, while those with very different energy densities will not. For example, if the solvent has a high energy density (say, water) this means that its component molecules are very strongly bound to one another (via, say, hydrogen bonding). If the intended solute (say, oil) has a very low energy density, that is, the molecules have no strong attractive forces, then those solute molecules will have a difficult time, with their weak intermolecular forces, of overcoming the strong intermolecular forces of the solvent to work their way between the solvent molecules.

Not only the magnitude but the character of the energy density is critical to solvation. The character is delinated by the force makeup of that density. From here comes the principle of 'like dissolves like'. These weak intermolecular forces fall broadly into three classes, determined generally by their character and strength. The weakest are dispersion forces, which are attractions between molecules that arise from transient fluctuations in electron density of the molecular orbitals. How powerful the dispersion forces are is indicated by the polarizability of the molecules involved, the polarizability being how easy it is for electric fields to induce transient dipoles in the molecule. The next class of forces are permanent polarities, which stem from differences in electronegativity of the atoms that constitute a molecule. These give rise to intermolecular attractions of medium strength. Finally, there are hydrogen bonds, which result from a hydgrogen atom, bonded to a highly electonegative atom like oxygen or nitrogen, being attracted to a highly electronegative atom on another molecule. These permanent molecular dipoles stem from unbalanced electron sharing between a hydrogen atom and its electrophillic bonding partner and may result in a molecule with no net dipole moment, but may still effect a considerable local attraction on other molecules with a polar nature, most especially those with similiarly highly positive hydrogen atoms.

Solvents are available with a wide variety of cohesive energy densities and force compositions. So wide, in fact, that for almost any two dissolvable substances, a range of solvents can be found that will dissolve one but not the other. For mixtures of a binary or ternary nature (such as those that were used in this work) the range of solvents will of course will be narrower, as something that dissolves all the components will need to be found. However, since the scintillating molecules generally are relatively similiar in their cohesive energy densities and component polarities (i.e., they are all relatively rigid, non-polar molecules), they will have approximately the same range of useable solvents.

2.6 Spin Casting and Baking Thin Polymer Films

Formation of the scintillator film is achieved via spin casting. This simple process involves the puddling of a small amount (a millileter or so for a 3 inch wafer) of solution in the center of the wafer, and then spinning the wafer at very high speed (several thousand rpm) to fling away the excess solution and coat the surface of the wafer uniformly, allowing the casting solvent to evaporate. Two properties of the scintillating film that are important: thickness and defect density. The thickness of the film determines the amount of energy the electrons deposit in the scintillator, and low defect density extends the area over which the electrons do not encounter unusual and thus deleterious scattering in the scintillating layer.

The thickness of the film is predicted to follow the equation

$$t = KS\left(\frac{\nu}{\omega^2 R^2}\right)^{1/3} \tag{2.12}$$

where K is a constant, S is the fraction of solids in the resist, ν is the kinematic viscosity of the resist, ω is the angular velocity of the spinner, and R is the wafer radius [31, 35]. While a thickness uniform to semiconductor processing standards is probably not necessary, this is relatively easy to achieve if the spin casting process is free of other problems.

With regards to defects in the films, several types are common: comets, lack of adhesion, and crystillization of solution components. Comets are caused primarily by particulates, either in the solution or on the substrate surface. These can be dealt with by using pure ingredients, following careful cleanroom procedures, and filtering the solutions before spinning.

Lack of adhesion finds its origin in the chemical incompatiblity of the solution and substrate surface, or in atmospheric contaminants, such as water or other solvents, which coat the substrate surface prior to spinning. Compatibility between the casting solvent or the base polymer and the substrate surface is controlled by weak intermolecular forces. For example, a highly polar solution (such as water) will likely not wet a highly non-polar surface (such as bare silicon), and hence will not spin well since all of the solution will be flung off during the spin, rather than coating the surface and allowing the solvent to evaporate. In addition to this, the base polymer might not stick well to the surface of the substrate, and so be discarded with the spin or flake off after application.

Crystillization of solution components depends the tendency of the components to crystallize in the first place, as well as upon the volatility of the solvent. A slowly evaporating solvent might give a component just enough time to crystillize, if it has any tendency to undergo that process. To deal with this, a more volatile solvent might be used, but this may leave a nonuniform film.

Finally, after films are spun, they must be baked to drive out any remaining solvent. The baking temperature must be high enough, and the baking time must be long enough, to allow for all of the solvent to volatilize. On the other hand, the bake must not be so long or so hot such that it causes degredation of the components of the spun film. Generally, monitoring the swelling of the film by using an ellipsometer to measure the decrease in thickness will give a good idea of the neccesary bake time at a certain temperature. Conversely, one must monitor the properties of the film (in the case of this work, the scintillation) to make sure that no degradation due to the heating has occured.

2.7 Integrating the Scintillator into an Electron-beam Resist Stack

Integration of the scintillator into an electron-beam stack is of key importance to SPLEBL. Ideally, we don't want to tie any property of the resist to the scintillator: we want to be able to spin it on, bleach the grid, expose, then remove it, all without affecting the electron-beam resist. This situation would not restrict a user of SPLEBL to any particular electron-beam resist, and thus would allow the greatest flexibility and foster acceptance of the method. In reality this decoupling of resist and scintillator cannot be so easily achieved, as we find that in many cases the two share both solvents and exposure wavelengths. Thus some subtlety is neccesary.

Solvent overlap can be illustrated by examining a selection of common high-resolution electron-beam resists, as shown in Table 2.1. As can be seen, chlorobenzene is a common electron-beam resist solvent. Unfortunately, this is exactly the solvent that was used primarily to spin scintillators. Indeed, the rigidity and non-polarity of the scintillating molecules (cf. Section 4.1) is similar to many of the common electron-beam resists (e.g., ZEP, CMS, and Calixarene). However, there is enough difference between the scintillating molecules and the electron-beam resists that it is conceivable that one would be able to find a discriminating solvent for each system.

The work in this thesis concentrated mostly maximizing brightness and contrast in the scintillators, and the issue of solvents was left to the sidelines. To overcome this solvent incompatibility a hard interlayer might be employed to integrate the scintillator into a stack without affecting the resist underneath. The possibility is illustrated in Figure 2-3c. This would be a viable research alternative, perfectly acceptable for the academic enviroment, but may not be attractive (or even suitable) for industry.

In addition to solvent compatibility, it is important that the light used to bleach the grid not expose the resist. This would not be a problem if one used 351 nm light, that used in the SNL's interference lithography setup. However, the scintillator contrasts achieved with that wavelength were mediocre, and it was found that a shorter wavelength – 220 nm – achieved a substantially better contrast (cf. Section 4.4 and 4.5). Unfortunately, this wavelength is known to expose electron-beam resists such as PMMA and CMS, as well as possibly others. Thus, when using such a short wavelength, one might make use of a scintillator-on-bottom and grid-exposure-first scheme in the SPLEBL stack, as illustrated in Figure 2-3d. In this case the scintillator is spun and exposed first, after which an interlayer and resist are laid down. Such a setup would require a trilayer pattern transfer process. This further complicates processing and is defect ridden, and so is generally undesirable, but may be neccesary depending on the contrast requirements of the SPLEBL implementation.

Finally, there would be further complications if it were desired to use an anti-reflection coating (ARC) to improve contrast in the Interference Lithography exposure of the scintillator. In the grating exposures shown

Resist	*Tone*	*Casting Solvent*	*Developing Solvent*	*Ref.*
PMMA poly(methyl methacrylate)	Pos	Chlorobenzene	IPA:MIBK	[28]
PBS poly(butene-1 sulphone)	Pos	MEK	2-pentanone : MIAK	[7, 6]
EBR-series poly(2,2,2-trifluoroethyl–chloroacrylate)	Pos	Methyl Cellosolve Acetate	IPA:MIBK	[39]
CMS poly(chloromethyl styrene)	Neg	Chlorobenzene	IPA:MIBK	[28]
ZEP-series poly α-chloromethacrylate co-α-methylstyrene	Neg	o-Dichlorobenzene or Diethylene glycol or Dimethyl ether	Xylene Alkyl Acetates	[29, 10]
Calixarene	Neg	o-Dichlorobenzene	Xylene	[13]
HSQ hydrogen silsesquioxane	Neg	MIBK	TMAOH	[42]

Table 2.1: A selection of high-resolution electron-beam resists

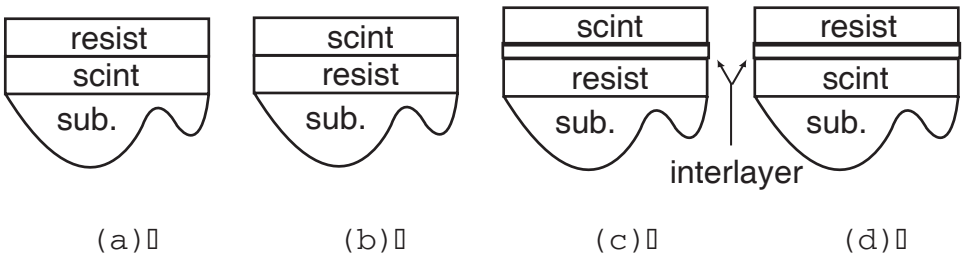

Figure 2-3: Possible SPLEBL stack configurations

at the end of this work, ARCs were used to achieve the highest possible contrast. A stack including an ARC, scintillator, and resist, plus associated interlayers, would be extremely complicated and highly undesirable. Thus, avoiding this at all costs is a worthy goal.

Chapter 3

Experimental Methods for Characterization of the Scintillators

This chapter describes the experimental methods used to characterize the scintillators. Scintillators were first prepared in solution, then spin-cast onto rigid substrates for testing by electron-beam. Bleaching with ultraviolet light was tested both by flood and interferometric exposures.

3.1 Preparation of Solutions

Solutions were prepared by mixing the specified ingredients, one by one, into the casting solvent. For all the scintillating solutions this casting solvent was chlorobenzene (C_6H_5Cl), except in those rare cases when we desired a more volatile solvent, in which case we used chloroform, $CHCl_3$. When bleachable salt solutions were prepared (cf. Section 4.5), water was used as the solvent.

All glassware was carefully cleaned with detergent and water followed by a 20 minute standard RCA clean. This consists of a solution five parts deionized water, one part hydrogen peroxide (H_2O_2), and one part ammonium hydroxide (NH_4OH), heated to 80^o C [35]. Magnetic, teflon coated stirbars were cleaned with isopropyl alcohol and methanol solvents.

Generally, the polymer was added to a set amount of solvent, 30 to 50 milliliters. Since the addition of the organic scintillators had a negligible effect on the spin coating, we were able to use these polymer-only solutions to adjust the concentration of the polymer to obtain the desired thickness at a reasonable spin speed. Typical quantities were 1 to 4 grams of polymer. After the polymer concentration was set, the rest of the components were added one at a time and allowed to dissolve completely. If any one component took longer than 24 hours to dissolve by stirring alone, the solvent was heated to about 90^o C. If this did not aid solvation, the concentration was lowered, or the material was removed from the trial.

3.2 Spin Casting and Baking

Solutions were spin cast on various sorts of substrates to produce thin films of the material of interest. For general tests of scintillators substrates were unprimed, virgin silicon wafers, fresh from the box. For a specific experiment investigating the effect of standing waves on contrast, scintillator was spun on top of ARC. Finally, in an experiment which measured the transmission curves for the water-soluble salts, UV-grade fused silica substrates were used.

Operationally, spinning involves placing the wafer on the spin chuck in the spinning machine, centering the wafer, setting the spin speed, dripping solution in a puddle in the center of the wafer, and finally activating the spinner for about thirty seconds. Solutions, despite being visibly free of particulates, were always passed through a polar or non-polar filter, as appropriate, as they were dripped onto the substrate. Typical thicknesses produced by a 4 g/30 ml polymer/solution spun at 2 krpm were generally between 500

and 900 nm, although concentrations and spin speeds were adjusted as desired to produce films of thicknesses between 50 nm and 1.2 μm.

Immediately after being cast, the films were baked at 90^o C in either a convection oven for 30 minutes, or on a hotplate for 1 minute.

3.3 Measurement of Scintillation

Once the scintillators were obtained in thin-film form by spin-casting solutions, their properties were probed by electron-beam.

Scintillation from organics is a notoriously weak phenomenon and requires high-gain detection. A rough calculation will illustrate this fact. We will calculate the number of photons produced by bombarding a scintillator with an electron beam, and then calculate the voltage this can produce across a detection resistor.

Consider the conditions of 100 pA of 5 keV electrons incident on a scintillating resist stack, with a thick scintillator on the bottom separated from a thin resist on top by an interlayer. Assuming that the electrons lose a small fraction of their energy in the resist and interlayer, say 500 eV, the majority of the energy is deposited in the scintillating layer. This gives us 4.5 keV deposited per electron. Multiplying by the number of electrons per second, and an optimistic conversion efficiency of 10%, we obtain the amount of energy per second deposited in the scintillating layer, or 2.77×10^{11} eV/s. If all that energy is deposited into one wavelength, say 420 nm (2.92 eV per photon), we will have 9.486×10^{10} photons/s emanating from the sample. If we optimistically assume we collect 4% of the light (optimisitic more especially because of total internal reflections and low substrate reflectivity), and optimisically assume the detector converts one in every four photons to an electron that can be measured, we will have 9.486×10^8 electrons/s, or 154.2 pA in our detector. Furthermore, since at least a 120 kHz bandwidth is needed for sparse sampling [22], and with a total system capacitance of no less than 50 pF (as an example, a standard scope runs at least 20 pF, plus coaxial cable connectors), this gives a maximum resistance of 166 kΩ for detection, and allows a readout of 25.5 μV. Thus a gain of 10^5 is needed for the best of cases. Realistically, a higher gain will be needed, somewhere in the neighborhood of 10^6 to 10^8.

A photomultiplier tube (PMT) is ideal for such an application, and is the instrument that were used. PMTs are high-gain, high-linearity, low-noise photon detectors with large bandwidths. They have been used specifically for scintillation detection for many years. Other options include externally amplified or avalanche photodiodes, but these are significantly noisier due to the smaller bandgap of the semiconductor materials (relative to the work function of a metal inside a PMT), and would only be neccesary where space or the presence of magnetic fields was an issue.

The operating principle of a PMT is illustrated in Figure 3-1. The photocathode converts photons into low-energy photoelectrons inside of the vacuum enclosure. These photoelectrons are then accelerated into the electron multiplier dynode structure, where each electron impact on each dynode produces several more electrons, producing an amplification cascade. Finally, the electrons are collected at the anode, where they can serve as a viable charge signal. Delay times depend on tube design, but are generally on the order of one hundred nanoseconds. Pulse broadening is usually in the tens of nanoseconds range.

Scintillator samples were spun on silicon and bleached with ultraviolet light (to be described in Section 3.4). Initial measurements of scintillation in response to an electron beam stimulus were taken in the LEO SEM chamber. A two-inch diameter focusing lens was used to collect light into a PMT, which is a type E258/E350 manufactured by EMI, purchased in 1968. [17, 34]. This setup is reported and described in the literature [18]. The PMT response is diagrammed in Figure 3-2 and shows a peak in sensitivity at 420 nm. Calculations indicate that about 0.6% of 2π steradians is collected into the PMT [17]. Measurements were conducted by blanking the beam, moving the field of view to a virgin area of the sample, and then unblanking the beam and measuring the PMT response with an oscilloscope. For the short times the beam was on (seconds) the scintillation signal was approximately constant, and so the magnitude of the signal served as the measure of the scintillation intensity.

As promising scintillator candidates emerged, measurements were shifted to the Raith 150 EBL system, purchased for the lab expressly for the demonstration of SPLEBL. James Goodberlet installed a Hamamatsu R6095 PMT in the vacuum chamber, along with a one-inch diameter lens to collect the light, a setup that will

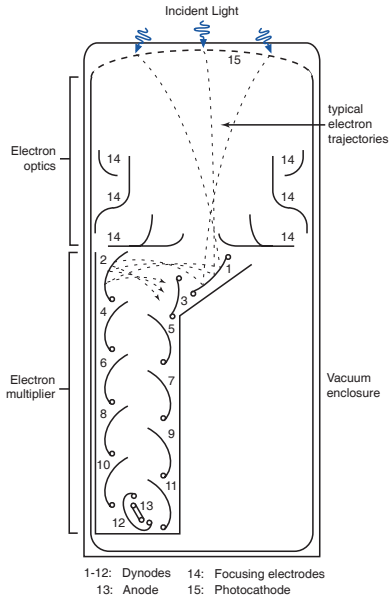

Figure 3-1: Schematic of a photomultiplier tube; adapted from [24, Figure 9.1]

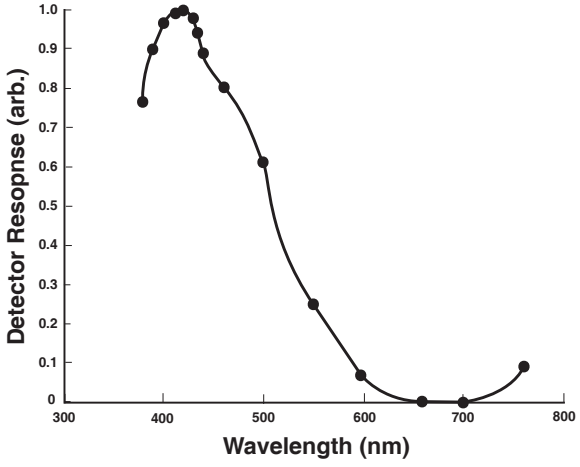

Figure 3-2: Response of the PMT installed on the LEO SEM; after data taken by J.G. Goodberlet [16]

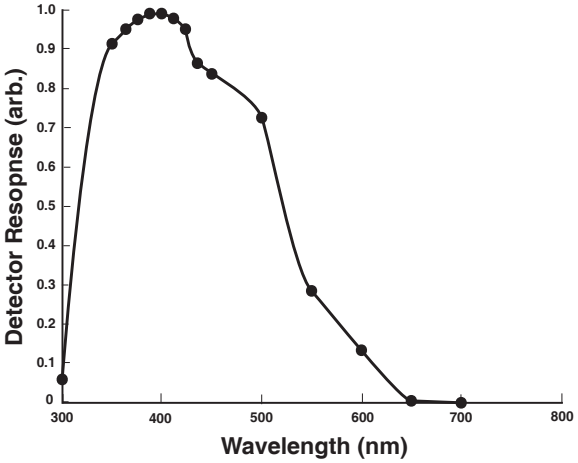

Figure 3-3: Graph of Hamamatsu R6095 photocathode response; after data from Hamamatsu datasheet for photomultiplier tubes R6094,R6095 [21]

be described in a future publication [17]. Solid angle calculations indicate that about 2.4% of 2π steradians is collected by the optics into the PMT. The Hamamatsu photocathode response is graphed in Figure 3-3, with a peak sensitivity at 420 nm as indicated by the datasheet.

It is important to note that, as a result of variations in quantum efficiencies of the photocathodes and dynodes in the PMT and an inexact knowledge of the accelerating voltages experienced by electrons inside focusing and electron multiplier stages, it is extremely difficult to correlate the electrical signals with a concrete number of photons arriving from the sample. This lack of knowledge is acceptable however, since a knowledge of the absolute scintillation efficiency is not neccesary for the work, all the scintillation output measurements taken here are relative to each other for the particular measurement device (i.e., LEO SEM or Raith 150 EBL tool). To properly compare measurements, the PMT was always set at the same value, 800 V. Additionally, it is important to note that even on the same tool, under the same set of experimental settings, with corrections for such variables as film thickness and beam current, scintillation measurements still were unable to be correlated to within 30%. This experimental variability is somewhat disturbing, and its source was never adequately identified, despite efforts to do so.

The SEM mode of both machines was used to conduct the measurements. In this mode the electron beam continuously raster scans the field of view. The field of view is generally made up of 512 by 512 sample points, and at best the low magnification used in this work (100X) corresponded to approximately a 350 micron square field of view. Thus the sample points were spaced about 750 nm apart. The horizontal cross-sectional diameter of the electron scattering volume should be much less than the Bethe range, which at 5 kV is a few hundred nanometers (although in general the larger the accelerating voltage, the smaller the diameter will be). Hence the excitation volumes at low magnifications do not overlap, and thus the scintillation signal does not depend on magnification, but only on beam current and accelerating voltage, as shown in Figure 3-5. This allowed the measurements to be normalized relative to current for a given voltage.

There were worries that perhaps scintillating samples would suffer from waveguide effects, that is, scintillations would be guided away from the detector by the thin film, and that emission from the edges of samples (which were generally small, irregularly shaped pieces with a surface area of approximately one centimeter square) could introduce a source of error into the scintillation measurement. Studies with samples of various sizes (variation of 75% area larger and smaller) and shapes (aspect ratios from 1 to about 50) were conducted to ensure that the scintillation measurement was insensitive to these factor.

One final test was conducted on all scintillators to provide an additional figure-of-merit. This involved measuring the *decay time* of the scintillator, which was a rough measure of how long the scintillation lasted under intense electron beam bombardment. This measurement was conducted by increasing the magnifi-

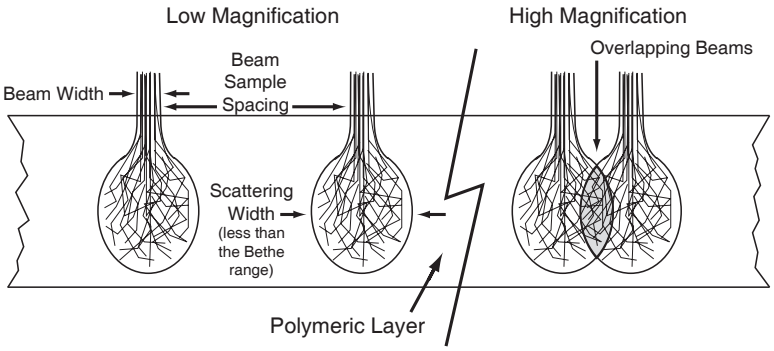

Figure 3-4: SEM mode used to probe for scintillation

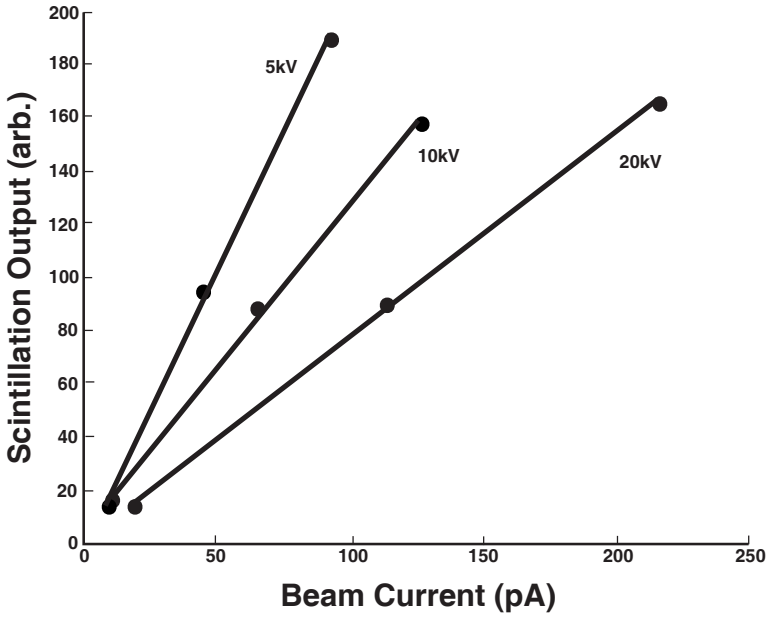

Figure 3-5: Linear dependence of scintillation signal on beam current for different accelerating voltages

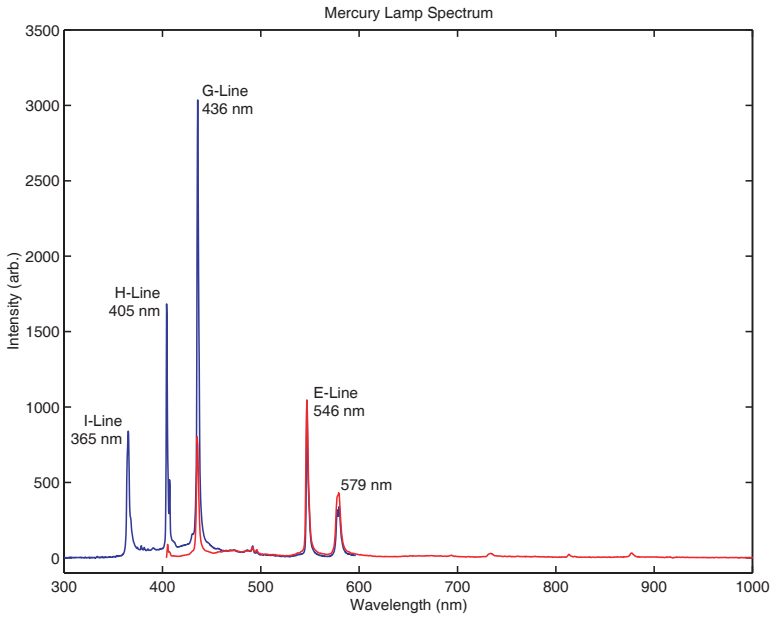

Figure 3-6: Spectrum of mercury lamp used for generic flood exposures; data was taken with two different gratings, and thus produced two spectrums which overlap from 400 to 600 nm

cation in SEM mode to the thousands, then leaving the field of view stationary and measuring the time it took the scintillation to decay to an arbitrary fraction of its initial value. At this high magnification the distance between sample spots is about 20 times closer, or about 40 nm. Thus the excitation volumes overlap significantly. We assumed simply that the decay time scales linearly with inverse of the current density, and so to normalize for beam current variations the magnification was changed according to the formula

$$M_{new} = \sqrt{\frac{i_{old}}{i_{new}}} \times M_{old} \tag{3.1}$$

Initial measurements of the decay time were taken at $i = 150$ pA and $M = 2000$ and so all subsequent measurements were normalized to these values. This figure-of-merit is quite rough, as measurements repeated under the same conditiosn found a significant standard deviation (20% or more). The source of this deviation could not be determined, as so this parameter was not relied upon heavily in choosing which scintillators to study further.

3.4 Area Bleaching with Ultraviolet Light

Flood exposures using a mercury lamp were used to quickly determine how well various scintillators bleached, and this was probed by electron-beam as described in Section 3.3. The spectrum of the lamp is shown in Figure 3-6. The procedure was simple: measure the power emitted by the lamp, and then expose several samples at different doses. For a Tamarak power of 4.7 mW/cm^2, samples were dosed conventionally for 0, 10, 20, 40, and 80 seconds. This exposure range generally showed the full bleaching response of the scintillators. There is some indication from the data that the doses may not have been well controlled, in that curve fits to different sets of data for identical scintillators yielded wildly varying values for the α parameter, or the characteristic bleaching dose. It is not clear whether this variation in dose was due to a variation in the actual bleaching dose of the scintillators, a miscalibration in the experimental setup, or an unaccounted for exposure.

Other bleaching tests were carried out at 220 nm and 260 nm using a HgXe lamp, as well as 325 nm [27]

with a HeCd laser, and 351 nm [32] Argon Ion laser. These tests were done to determine if the bleaching response for these wavelengths differed from that induced with the mercury lamp. It was found that the 220 and 260 nm exposures were not phenomenologically different from each other, but showed much more profound bleaching than the 351 nm and mercury lamp exposures. Thus, detailed flood exposures were carried out at 220 nm, 351 nm, and mercury lamp wavelengths.

Evidence for the necessity of exposure to atmosphere (and hence oxygen) for bleaching at mercury lamp wavelengths was obtained by attempting to bleach films with thin (30 nm) layers of evaporated oxide on top. Films did not bleach through this oxide layer, even though simulations indicated that a significant amount of light passed into the scintillator. As oxide is a barrier to atmospheric gases, it was concluded that exposure to atmosphere is neccesary for bleaching (specifically, from photochemical considerations, exposure to oxgyen).

Several experiments were conducted to determine if the films were bleaching all the way through. These experiments involved changing the thickness of the films and looking for a change in contrast. Scintillators #20b and #6 (cf. Table 4.1) were tested at thicknesses from 200 nm to 1 micron and showed no significant change in contrast. This was to be expected, since optical absorption coefficients of all the various scintillator constituents indicate that most of the UV light should pass right through the film, thus exposing the film relatively uniformly all the way through. There was some question of the presence of a standing wave for the coherent sources, which is why an ARC layer was used for some of those exposures. This issue is dealt with in Section 4.5.

Finally, it must be noted again that the measurements of scintillation were never extraordinarily repeatable. This was a source of continual consternation, and still lies unexplained.

3.5 Bleaching & Imaging a Fiducial Grid

The final test of any scintillator evaluated in this work is its use in the production of a fiducial grid bleached by interference lithography. For most purposes, this demonstration can be reduced to the bleaching of a fiducial grating, as a grid is produced by the sequential exposure of two gratings, one orthogonal to the other, and requires merely an adjustment of the dose. It should be noted that all bleaching and imaging of gratings presented in this were carried out under the cheerful supervision of Todd Hastings.

First attempts to produce fiducial gratings used a 325 nm laser with a Lloyd's mirror. This setup is described in the literature [27]. To decide on the dose to produce a grating, we used the Lloyd's mirror system contrast [27] to determine the ratio of peak-dose to valley-dose (i.e., the ratio between areas with constructive and deconstructive interference). Then by reference to bleaching curves taken either by mercury lamp (as described in the last section, 3.4) or by the 325 nm laser itself, we decided how much degradation in peak scintillation was acceptable, given the Lloyd's mirror interference lithography contrast. Generally this degradation of peak scintillation was set to the arbitrary value of 5%. This then set the exposure dose.

Gratings were also bleached with the Space Nanostructures Laboratory's (SNL's) interference lithography setup [32]. This setup uses a 351 nm laser and requires the full assistance of James Carter to operate. Similar procedures to calibrate the dose were used for this system. Anti-reflective coating layers are often used in this system to improve the exposure contrast, and so these were investigated for the scintillators as well (cf. Section 4.5).

Either Todd Hasting's sparse-sampling procedure was used to image fiducial grids produced in the scintillators [23], or the grids were imaged directly. Sparse-sampling consists of probing the scintillator at discrete locations within the e-beam field, with a period larger than that of the grid, this method produced a moire pattern which allowed the period and contrast of the grid to be measured. The method was implemented by Todd Hastings on the Raith 150 EBL tool, and the algorithms and step-by-step procedures are detailed in his doctoral thesis [22]. In this work it is taken as a set measurement procedure, with no further elaboration.

Chapter 4

Evaluation of Scintillator Performance

This chapter presents the details of the various materials sytems investigated as possible scintillators. The first two sections describe standard (already existing in the literature) and novel systems, respectively, and the reasons for investigating them. The next two sections present the data on relevant figures-of-merit for the various scintillating systems, and presents detailed data on select exceptional systems. Section 4.5 sketches a few schemes that were explored to increase the contrast of various systems. Finally, the bleaching and imaging of a scintillating fiducial grid, the nominal goal of this work, was demonstrated. To be sure, achieving less than a nanometer pattern placement accuracy with a scintillating grid is the ultimate goal, but this achievement is dependent on the full development of SPLEBL, which is beyond the scope of this thesis.

4.1 Standard Scintillating Systems

At first, prospective scintillating systems were selected from the literature [5]. Standard plastic systems, in use since 1950 [33], and still produced commercially [11], consist of an alykyl benzene polymer host, a strongly emissive primary organic flourophore, and an efficient secondary organic flourophore serving as a wavelength shifter. Many systems also contain an additional component (naphthalene) that assists in energy transfer from the host to the primary scintillator. Specific data on the performance of the various systems tested is summarized in Section 4.3. The benchmark was the first system formulated: a poly(methyl methacrylate) (PMMA) host with naphthalene (8 wt%), anthracene (2.5 wt%), and POPOP (2.5 wt%). The naphthalene-anthracene-POPOP scintillator combination also served as a benchmark system with which to compare the efficacy of new polymer hosts, as appropriate.

Choice of polymer host was dictated by the efficiency of the scintillating plastic base (i.e., how bright the final scintillator was for given primary and secondary scintillators). Polymeric hosts that were tested were poly(methyl methacrylate), polystyrene, poly(vinyl toluene), poly(vinyl xylene), and poly(vinyl napthalene), all illustrated in Figure 4-1. PMMA was the first polymer tested, as this is a common resist for electron-beam lithography. It was found, in agreement with the literature [5, Chapter 9] that, with the same concentrations of scintillators, the polystyrene based scintillators performed much better than PMMA, being two to four times as bright. Moreover, the addition of methyl groups to polystyrene (to form poly(vinyl toluene) or poly(vinyl xylene)) increased the observed efficiency by another factor of 30%. This increase is attributed to a decrease in the polymer's excitation energy and an increase in the oscillator strength of the excited transition, which results from electron donation into the ring system by the substituted methyl groups [5, § 9.11]. Poly(vinyl naphthalene) was found to be a little less than twice as bright as the PMMA based scintillator, but its damaging time was the longest recorded. The polystyrene related polymers were also found to have much longer damaging times than PMMA.

Choice of a secondary scintillator was constrained primarily by location of the detectivity peak of our systems's PMT tubes (cf. Section 3.3), located at 420 nm. The secondary scintillator used for nearly all of these standard plastic scintillating solutions was POPOP, although dimethyl POPOP was tested in a few instances (see Figure 4-2). Happily, POPOP (1,4-Bis(5-phenyl-2-oxazolyl)benzene) is one of the most

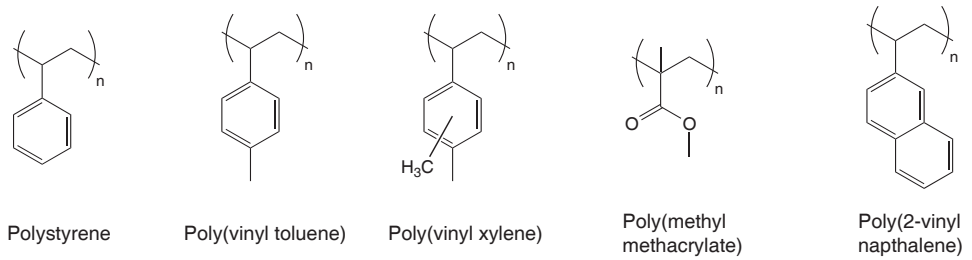

Figure 4-1: Standard polymers tested

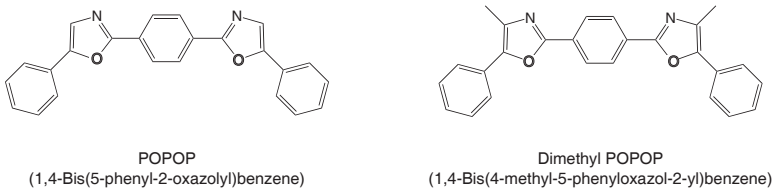

Figure 4-2: Secondary scintillators tested

efficient secondary scintillators known [5].

Choice of primary scintillators was constrained by their brightness [5] and emission spectrum [4]. The emission spectrum was required to overlap significantly with that of the secondary scintillator, POPOP. If a primary scintillator's main emission peak was at 420 nm, a secondary scintillator was not used. Primary scintillators that were tested are shown in Figure 4-3. These included anthracene and two of its derivatives, dimethyl anthracene and diphenyl anthracene, para-terphenyl, para-quaterphenyl, tetraphenyl butadiene, and two oxadiazole derivatives, Bis-biphenyl and phenyl-biphenyl.

The anthracene derivatives (9,10-dimethyl and 9,10-diphenyl) and dimethyl POPOP were tested because it was thought they might prove more resistant to electron beam damage, as the substitutents protected the most reactive sites of those molecules. As can be seen from the data in Section 4.3, these substitutents did not provide any significant additional resistance. It is likely that this is due to the electron-beam damage being molecule nonspecific, that is, it damages everything equally due to its high energy. In this case degradation of the polymer would account for a significant portion of electron-beam induced bleaching, an idea which led to the testing of more stable polymers (described in Section 4.2).

For certain primary scintillators, it is noted in the literature that the addition of large amounts of naphthalene increases the efficiency of the solutions by absorbing energy from the polymer and transferring it efficiently to the primary scintillator [14]. Naphthalene was not used in p-terphenyl based solutions, as the similarity of their spectra does not allow for energy transfer [5, § 8.3.2].

Not all primary scintillators were tested with all the various polymer hosts. As already noted, the standard combination was naphthalene-anthracene-POPOP, which was a benchmark system that was tested with all the standard polymers. Typical concentrations of solutes which, according to the literature, yielded peak scintillation efficiencies, were in the range of 2.5 to 5 wt%. This is shown in Figure 4-4, taken from reference [5]. Those systems containing naphthalene generally contained about 8 wt%, or about 1.6 to 3.2 times as much naphthalene as compared with the primary or secondary scintillator.

When the concentration of some solutes was raised beyond a certain point, crystallization occured during spin coating. Figure 4-5 shows the formation of p-terphenyl grains in poly(vinyl toluene) as the concentration is raised past a critical level.

Approximately thirty different standard scintillating systems were tested. Figures-of-merit concerning brightness, damaging time, and bleachability were measured in survey tests, and are summarized below in

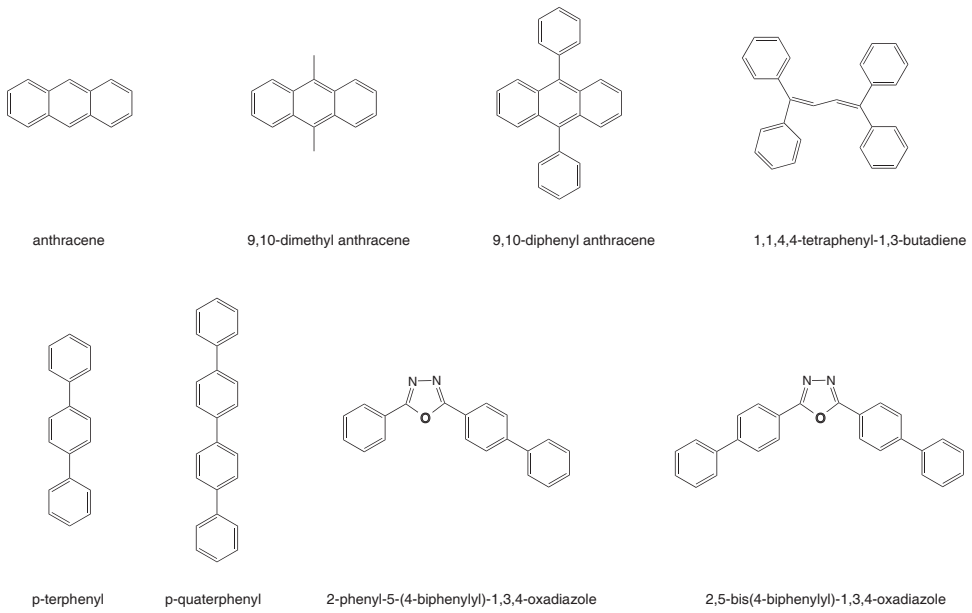

Figure 4-3: Primary scintillators tested

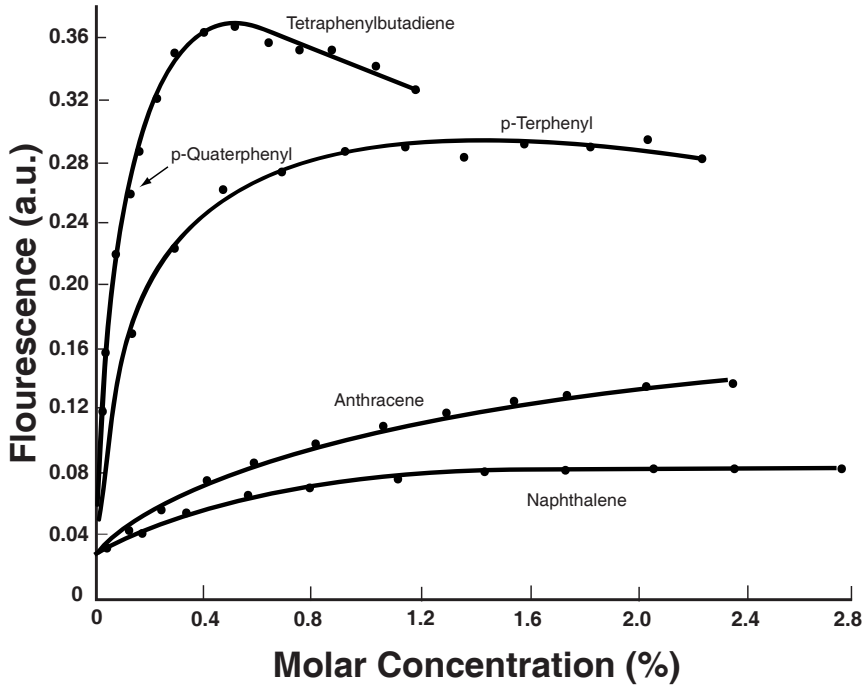

Figure 4-4: Polystyrene solutions excited by β-particles; after [37, Figure 1], with extraneous components omitted for clarity

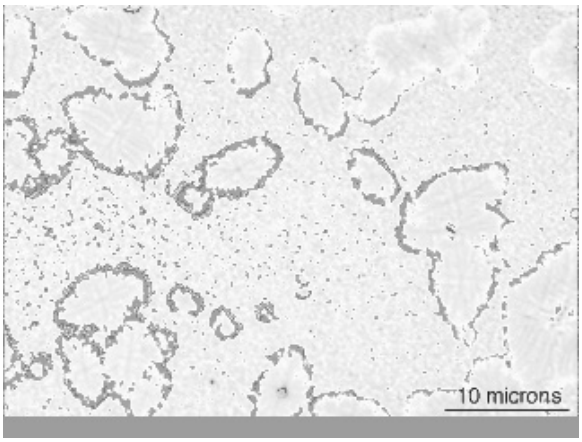

Figure 4-5: p-Terphenyl grains formed during spin coating a Poly(vinyl toluene) film

Section 4.3. The field of competitors was narrowed by reference to these figures, and this is discussed below in Section 4.4.

4.2 Novel Scintillating Systems

In addition to scintillating systems derived from the literature, a number of novel scintillating systems were tested. Chlorine-substituted polystyrene and poly(vinyl toluene) were tried with the hope of increasing the brightness of the solutions. Poly(vinylbenzyl chloride) and poly(4-chlorostyrene) were noted to be better electron beam resists [28, § 5-4-1] than either PMMA or polystyrene. It was posited that this increase in sensitivity was due in part to a heavier electron scattering cross-section of the resist, attributable to the large chlorine atom, i.e., more efficient energy absorbtion by the polymer. This, it was hoped, would correlate directly with an increase in energy absorption and transfer to solutes, hence increasing brightness. To investigate their efficiencies, both polymers were tested with the naphthalene-anthracene-POPOP benchmark system. Contrary to expectations poly(vinylbenzyl chloride) was found to have a brightness about one-third of the benchmark PMMA-based scintillator and poly(4-chlorostyrene) based scintillator did not emit appreciably at all.

Two specially-sythesized polymers from the Swager group were tested, the Jye [44] and Zhengguo [45] polymers (illustrated in Figure 4-6). These polymers were not expected to bleach with ultraviolet light by themselves; rather, it was planned that a singlet-oxygen sensitizer, Rose-Bengal, would be added to oxidize the polymer under irradiation in air. It was found that the Jye polymer formed clumps after spinning on silicon from Chlorobenzene, and so was not usable. The Zhengguo polymer spun nicely, and showed no sign of bleaching under mercury lamp exposure, and was reasonably bright (about 2.5 times PMMA/NAP) but its resistance to electron-beam induced damage was quite poor, and so was eliminated as a candidate.

The Swager group also suggested that poly(vinyl chloride) (PVC) be added to the Zhengguo polymer, to increase its resistance to electron-beam irradiation (PVC is known to dissolve molecules with similar structures). However, the two polymers separated upon spinning, and since neither fast spins nor a highly-volatile solvent (chloroform) were able to fix the problem, uniform films of the mixture could not be produced. A poly(vinyl chloride) based system with naphthalene, anthracene, and POPOP also suffered from the same problem, and so this polymer was eliminated from further consideration.

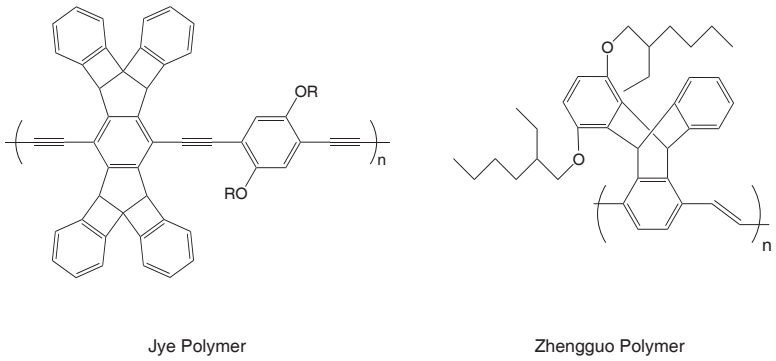

Figure 4-6: Novel electronic polymers tested

4.3 Survey Data on Performance of Systems

From the range of systems tested, a select few were singled out for further study based on a few figures-of-merit. Data regarding these is collected in Table 4.1. Experimental procedures involved mixing the solutions, spinning and baking the solutions to form thin films, flood exposure to bleach, and electron-beam probing to measure output and damaging time, all as described in Chapter 3.

Base concentrations used in these mixtures were generally 2.5 to 4 grams of polymer (depending on the desired spin speed and film thickness) in 30 milliliters of chlorobenzene, with 0.0625 to 0.1 grams of both the primary and secondary scintillators (i.e., corresponding to 2.5 wt% of polymer), in addition to 0.2 to 0.32 grams of naphthalene (i.e., 8 wt% of polymer), if applicable. Some solutions contained more primary scintillator, as indicated in Table 4.1.

A bleaching curve that might be obtained via these methods is shown in Figure 4-7. An exponential curve was fit to each data set using a least squares method, according to the equation

$$I(\delta) = A \exp\left(-\delta/\alpha\right) + B \tag{4.1}$$

where δ is the bleaching dose, α is a measure of how quickly the scintillation bleaches with dose, A is the bleachable part of the scintillation, and B is the unbleached background. In Table 4.1 below, the brightness is equivalent to $A + B$, and contrast is defined as $(A + B)/B$.

4.4 Detailed Data on Satisfactory Systems

After all systems were surveyed, several of the highest performers were selected for further study. Systems were evaluated with regard to three figures-of-merit: brightness, bleachability (i.e., contrast), and damaging time.

The brightest systems were #18 and #20b, both with reasonable damaging times. The poly(vinyl xylene) based #18 was not considered further as it had very poor contrast (although a very long damaging time). Moreover it was not readily available commercially, and had to be specially synthesized [8]. The poly(vinyl toluene) based #20b with p-terphenyl primary scintillator was considered the most promising candidate of all the scintillators due to its high brightness, short damaging time, and reasonable contrast. Furthermore, poly(vinyl toluene) (also known as poly(4-methyl styrene)) is low cost and readily available, being the most commonly used polymer base for commercial scintillators.

The systems with the longest damaging times were those from the poly(vinyl naphthalene) based #5 class. While these scintillators were about half as bright as #20b, they had an excellent contrast. The systems with the best contrast were the poly(vinyl naphthalene) based #5b and the polystyrene based #6.

These three scintillators (#5b, #6, and #20b) were chosen for detailed investigation, along with the original scintillator #1 (the benchmark PMMA based system) for comparison. The spectra of these components

PVC	=	poly(vinyl chloride)	PVN	=	poly(vinyl naphthalene)
PMMA	=	poly(methyl methacrylate)	PS	=	polystyrene
PVT	=	poly(vinyl toluene)	PVX	=	poly(vinyl xylene)
PVBCl	=	poly(vinyl benzyl chloride)	P4ClS	=	poly(4-chloro styrene)
anth.	=	anthracene	N	=	naphthalene
TPB	=	tetraphenyl butadiene	PBD	=	phenyl biphenyl oxadiazole
DBO	=	dibiphenyl oxadiazole	NM	=	Not Measured

#	*Host*	*Primary Scintillator*	*Secondary Scintillator*	*N?*	*Brightness (arb.)*	*Damaging Time (sec)*	*Contrast*
3	-	Jye Polymer	-		not spinnable		
4	-	Zhengguo Polymer	-		660	0.6	1
10	PVC	Zhengguo Polymer	-		not spinnable		
11	PVC	anth.	POPOP	√	not spinnable		
5a	PVN	anth.	POPOP		422	5.9	2.8
5b	PVN	anth. (×4)	POPOP		414	6.3	3.2
5c	PVN	anth. (×8)	POPOP		not spinnable		
5d	PVN	anth. (×10)	POPOP		not mixable		
14	PVN	diphenyl-anth.	-		534	4.9	1
1	PMMA	anth.	POPOP	√	250	1.2	2.2
2	PMMA	dimethyl-anth.	POPOP	√	74	1.5	< 1.5
6	PS	anth.	POPOP	√	565	2.7	3.8
7	PS	dimethyl-anth.	POPOP	√	397	2.8	2.4
8	PS	dimethyl-anth.	dimethyl-POPOP	√	666	2.9	2.8
9	PS	Zhengguo Polymer	-		not spinnable		
12	PS	p-quaterphenyl	POPOP		574	2.8	2.9
15a	PVT	anth.	POPOP	√	672	2.8	2.4
15b	PVT	anth. (×10)	POPOP		not spinnable		
17	PVT	anth.	dimethyl-POPOP	√	649	3.5	2.7
16	PVT	dimethyl-anth.	dimethyl-POPOP	√	430	2.8	2.2
13	PVT	diphenyl-anth.	POPOP	√	287	2.9	2.2
19a	PVT	TPB	POPOP	√	414	2.7	2.4
19b	PVT	TPB (×5)	POPOP	√	340	2.7	2.4
19c	PVT	TPB	-	√	375	6.7	1
19d	PVT	TPB (×5)	-	√	295	4.1	1
20a	PVT	p-terphenyl	POPOP		583	2.8	2.6
20b	PVT	p-terphenyl (×5)	POPOP		900	3.6	2.4
20c	PVT	p-terphenyl (×10)	POPOP		785	2.8	2.2
21a	PVT	PBD	POPOP	√	589	2.5	1.9
21b	PVT	PBD (×5)	POPOP	√	537	2.8	1.2
22a	PVT	DBO	POPOP	√	671	2.2	1.9
22b	PVT	DBO (×5)	POPOP	√	not spinnable		
22b	PVX	anth.	POPOP	√	827	6.6	1.3
23	PVBCl	anth.	POPOP	√	88	1.6	NM
24	P4ClS	anth.	POPOP	√	< 10	NM	NM

Table 4.1: Survey data of all scintillating systems tested

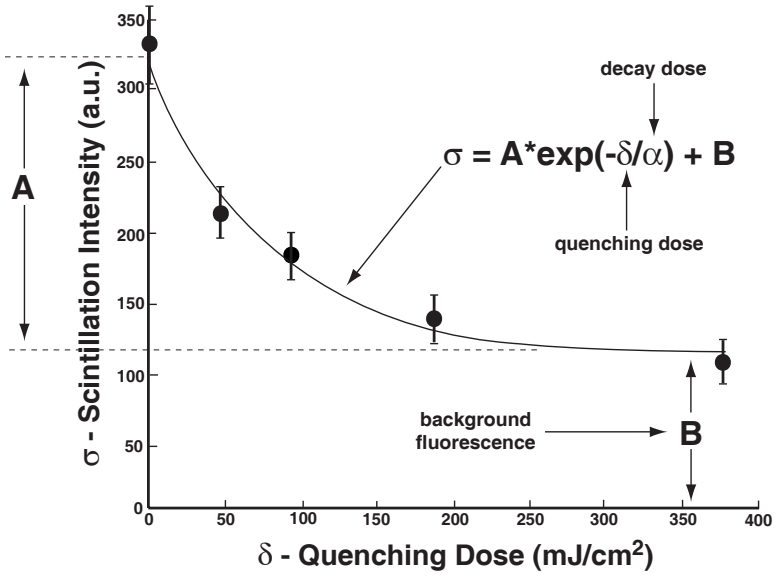

Figure 4-7: Generic bleaching curve with fit equation

are shown in Figure 4-8. The p-terphenyl based scintillator had an additional advantage over the anthracene based scintillators, in that the spectrum of the p-terphenyl is well separated from that of POPOP. This made the scintillator amenable to optical filtering to improve the contrast, as indicated in the Section 4.5.

Detailed bleaching data on the different scintillator components with a mercury spectrum are shown in Figures 4-9 and 4-10. Interestingly, the only component that bleaches significantly with the mercury lamp spectrum is POPOP. This is in contrast to bleaching at 220 nm wavelength, which will be examined in Section 4.5.

Detailed data on the bleaching curves are shown in Figure 4-11. Scintillators were also tested in detail at 351 nm wavelength, which is the wavelength of the SNL interference lithography system. This data is shown in Figure 4-12 and summarized in Table 4.2. It would be expected that the contrasts measured with these two techniques would be approximately the same, as the mercury spectrum (cf. Figure 3-6) has a line at 365 nm. As can be seen, Scintillator #1 has the highest contrast measured. However, this does not neccesarily translate into a better signal, since the measurements of that scintillator were quite noisy due to the high PMT gain neccesary to see the signal. The other three scintillators, especially #20b, were much brighter, and consequently had a much cleaner signal. The requirements of SPLEBL with regard to a noise vs. contrast tradeoff will depend on its particular implementation, which will be covered in future work [22]. For the moment, we will be satisfied that alternatives (i.e., high noise and contrast vs. low noise and contrast) exist.

The careful observer will note that the contrasts quoted in Table 4.2 do not match those quoted in the scintillator survey, Table 4.1. It is unclear why this is the case. It is possible, with the survey, that there were experimental inconsistencies over time (as it was conducted over the span of many months) that have not been accounted for, such as incorrectly calibrated doses that would result in ill fitted curves to the data and incorrect contrast measurements. Fortunately, the detailed data that was taken with great care (Figure 4-11 and 4-12) are reasonably self-consistent, as we might expect from the mercury lamp spectrum containing a line at 365 nm.

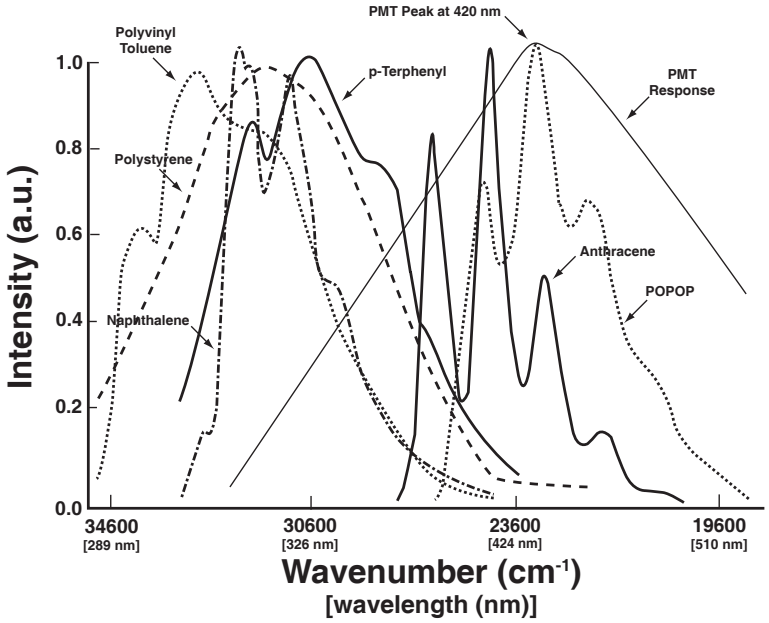

Figure 4-8: Various scintillator component emission spectra: polystyrene, poly(vinyl toluene), naphthalene, anthracene, p-terphenyl, and POPOP, along with PMT response (arb. units)

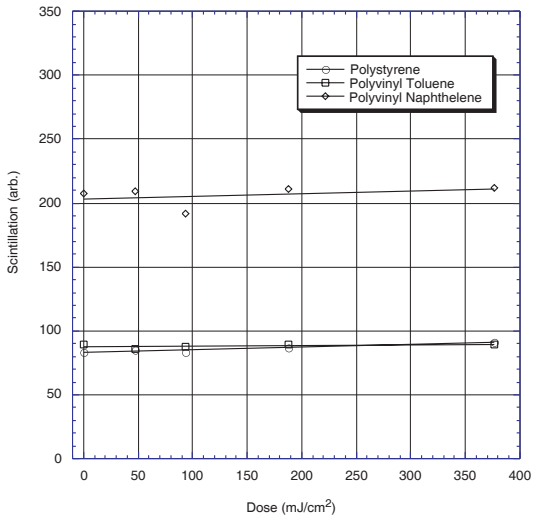

Figure 4-9: Bleaching of base polymers with mercury lamp

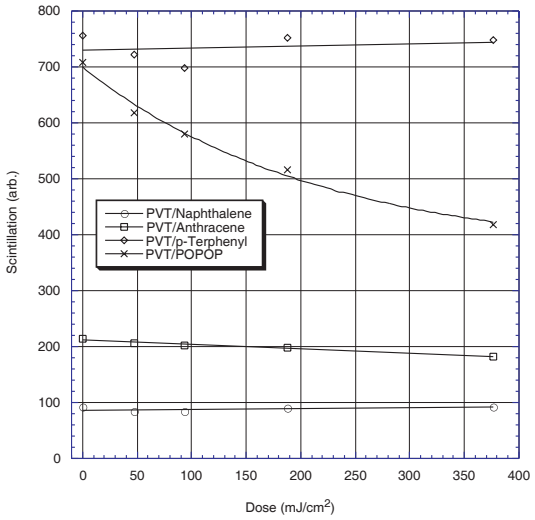

Figure 4-10: Bleaching of scintillating components with mercury lamp

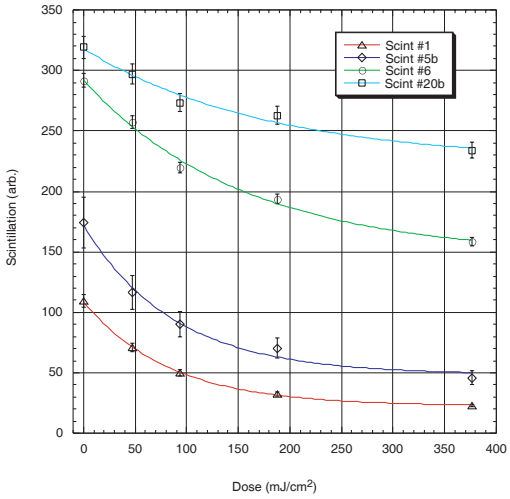

Figure 4-11: Detailed data on scintillators #1, #5, #6 and #20b, bleached with mercury lamp light

Scintillator	Merc. Contrast	351 nm Contrast
#1	4.2	3.3
#5b	3.5	3.5
#6	2.0	2.3
#20b	1.4	1.4

Table 4.2: Contrasts of the best scintillators with mercury lamp and 351 nm bleaching

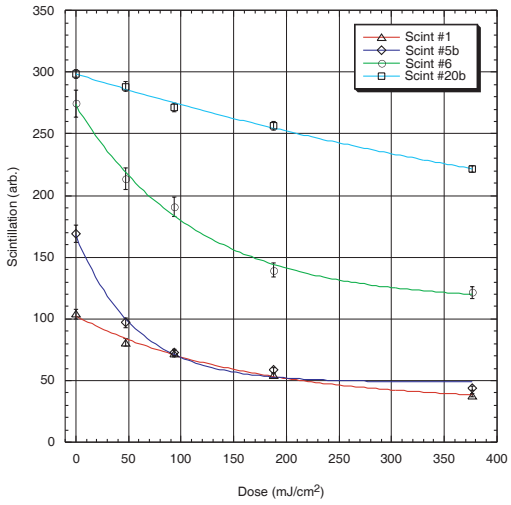

Figure 4-12: Detailed data on scintillators #1, #5, #6 and #20b, bleached with 351 nm light

4.5 Contrast Enhancement Schemes

As can be see from Table 4.1, contrasts for even the best scintillators are quite low, no higher than 4. Furthermore, initial attempts to bleach gratings in the scintillator indicated that contrasts of fine-period gratings might be much lower than the contrast measured by the flood exposure technique, for reasons that are not yet fully understood (see Section 4.6 for a detailed discussion of possible explainations). As it has been shown that high contrast is essential to achieving accurate pattern placement in SPLEBL [15], a significant amount of effort was expended trying different schemes to improve the contrast of the scintillators.

First, Swager's group suggested using an optical filter to discriminate between peaks of the p-terphenyl and POPOP spectra in scintillator #20b. As can be see from Figure 4-10, POPOP is the only component that bleaches significantly, and Figure 4-8 indicates that POPOP's spectral peak is distinct from that of p-Terphenyl. A high-pass wavelength filter with a sharp turn-on at 400 nm was installed in the Raith 150 system. Tested on scintillator #20b, it was found to increase the contrast from 1.6 to 2.1. This was a mild improvement, but hardly outstanding.

Another scheme, suggested by the Swager group, was the introduction of Rose-Bengal dye as an additive [40]. When exposed to ultraviolet light, Rose-Bengal dye produces singlet oxygen, a strong oxidant, which would be expected to aid bleaching. The dye can then be deactivated by exposure to HCl vapor, as illustrated in Figure 4-13. For this experiment, we used a bis(triethyl ammonium) salt of Rose-Bengal. Unfortunately no difference or improvement in contrast was observed.

Bleachable salts were also investigated as possible contrast enhancement schemes. This work was based on the CEL (contrast enhancement layer) scheme devised by Griffing and West in 1983 [19, 20, 43]. The heart of the idea is to spin a layer on top of the scintillator which is bleachable at the exposure wavelength, thus resulting in an increase in effective contrast of the light that reaches the bottom layer. This scheme would result in a small 'shelf' in the bleaching curve of the underlying scintillator, as shown in Figure 4-14. This scheme would protect against a low contrast interference lithography exposure (to which the scintillator, with its exponential decay in output on dose, would be quite sensitive). Two diazonium salts, p-morpholinobenzene diazonium double salt, and N,N-dimethylaminobenzene diazonium double salt [43, 41, 12] were chosen according to their documented wavelength sensitivities and the fact they are water soluble (which would aid their application), and were synthesized by Dr. Bronstein [9]. The salts were spun in a matrix of the water soluble polymer poly(N-vinyl pyrrolidone). All of these components are illustrated in Figure 4-15. The absorbance band bleaching of these salts with mercury lamp light at an arbitrary concentration

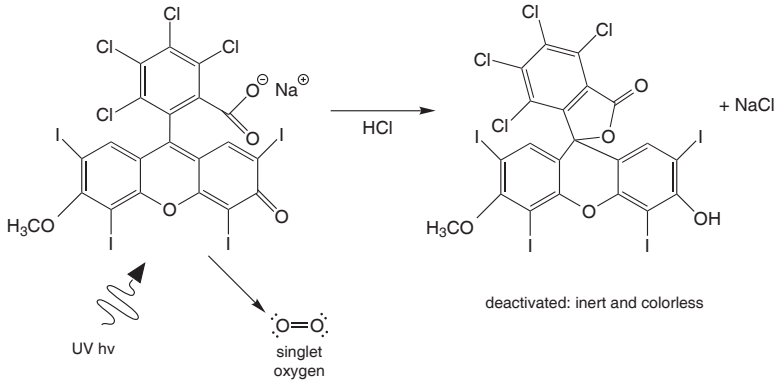

Figure 4-13: Rose Bengal singlet oxygen production and protonation reaction to deactivated form

Scintillator	Contrast
#1	74
#5b	32
#6	2.7
#20b	13.8

Table 4.3: Contrasts of the best scintillators at 220 nm bleaching

was measured as shown in Figure 4-16. Spinning the water-solution on top of the scintillator proved to be somewhat troublesome, and eventually it was required to use an extremely thin (1 to 4 nm) oxide interlayer to induce adhesion. Nevertheless the scintillator showed the proper CEL action, as shown in Figure 4-17.

Additionally, bleaching with wavelengths shorter than that of the mercury spectrum was tried as a way to increase contrast. The seed idea for this approach was the possibility that the polymers would degrade (as PMMA is wont to do) under the more intense exposure, thus lowering the background. Bleaching at 220 nm and 260 nm was carried out with the OAI Hybralign Series 400 exposure tool. This proved to be the most effective way of improving the contrast, with fully bleached samples having almost no detectable scintillation. Measured contrasts at 220 nm are shown in Table 4.3. Due to noise in the measured signals, the higher values of contrast (those greater than 10) are accurate only to within +/- 30 %. Bleaching of individual components at 200 nm was measured as shown in Figures 4-18, 4-19, and 4-20. It can be seen that polystyrene did not bleach perceptibly, so that polymer was used as the base to test the bleaching character of other scintillating components. In contrast the mercury lamp case, every single component and polymer (except polystyrene) exhibited strong bleaching.

Detailed bleaching curves of the different scintillators at 220 nm were taken as well, shown in Figure 4-21. Detailed bleaching curves for the highest performing scintillators at 220 nm is shown in Figure 4-21.

Finally, it was hypothesized that using an ARC (anti-reflection coating) in the interference lithography exposures would assist in producing higher contrast gratings through the elimination of standing waves [30]. Data testing this hypothesis (to be contrasted with Figure 4-12) is shown in Figure 4-22. Flood contrast figures are listed in Table 4.4. The scintillators showed no significant increase in contrast with the ARC..

4.6 Bleaching & Imaging a Fiducial Grid

Finally, once the scintillator development was concluded, it was desired to demonstrate the nominal goal of this work, the production of a scintillating fiducial grid. In a high contrast interferometric exposure, the production of one orthogonality of the grid is functionally equivalent to production of full a grid, and thus

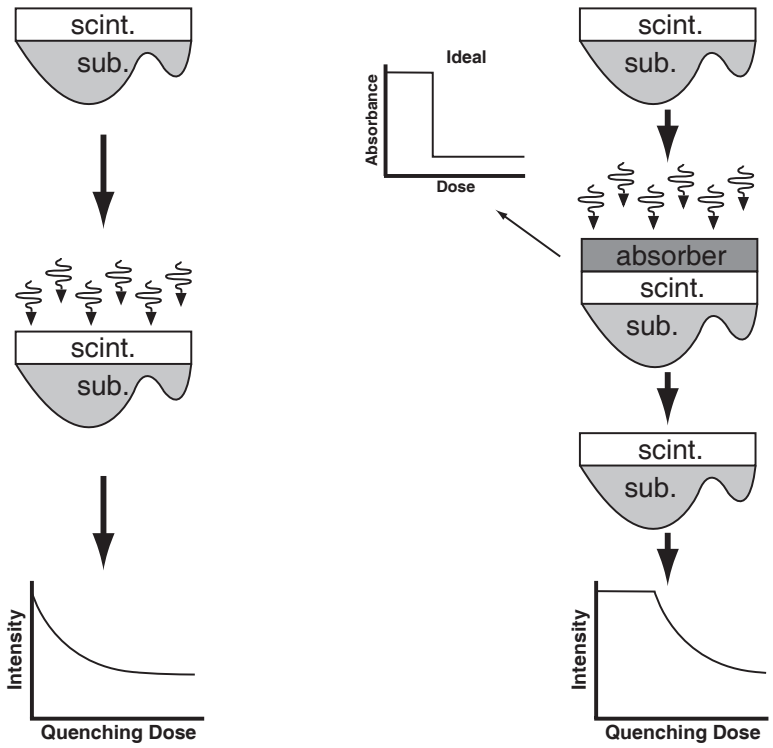

Figure 4-14: Concept of the contrast enhancing layer as applied to bleaching scintillation

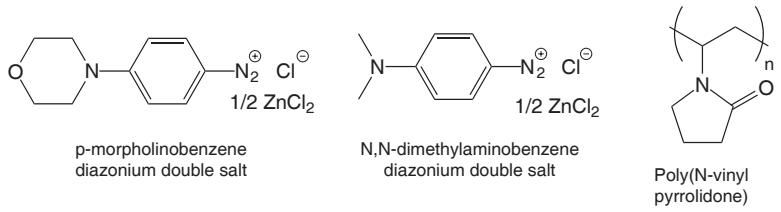

Figure 4-15: Bleachable diazonium salts and poly(N-vinyl pyrrolidone)

Scintillator	351 Contrast	351 Contrast with ARC
#1	3.3	3.3
#5b	3.5	3.5
#6	2.3	2.5
#20b	1.4	1.4

Table 4.4: Contrasts of the best scintillators at 351 nm bleaching, with and without an ARC

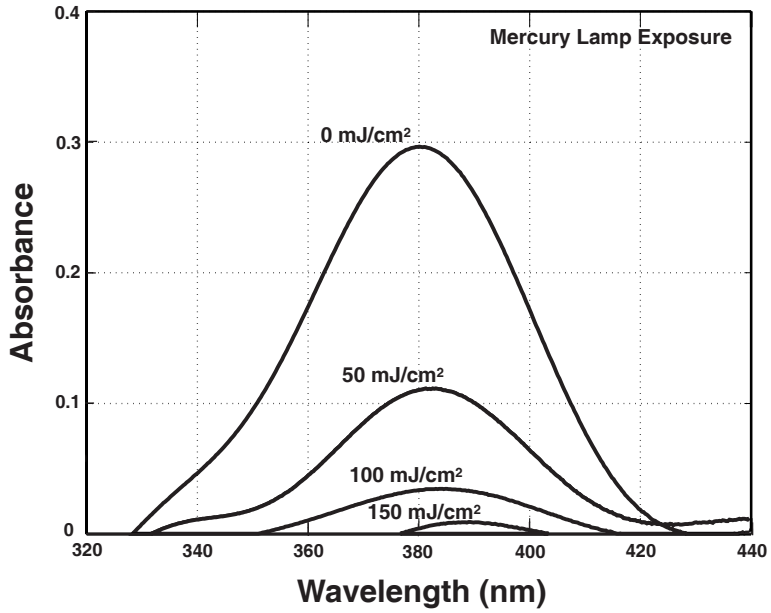

Figure 4-16: Diazonium salt absorbance bands at an arbitrary concentration, showing bleaching with increasing mercury lamp dose

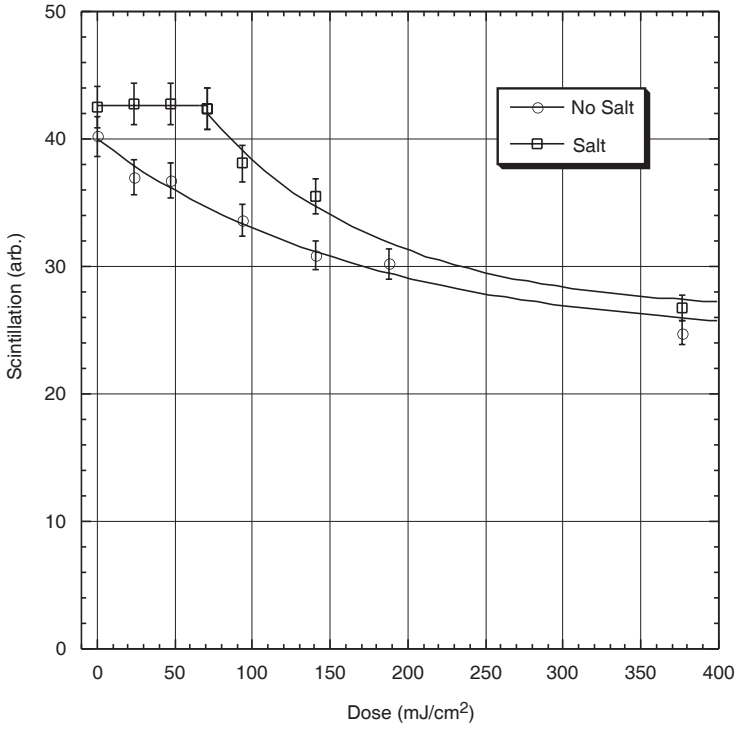

Figure 4-17: Demonstrated CEL action

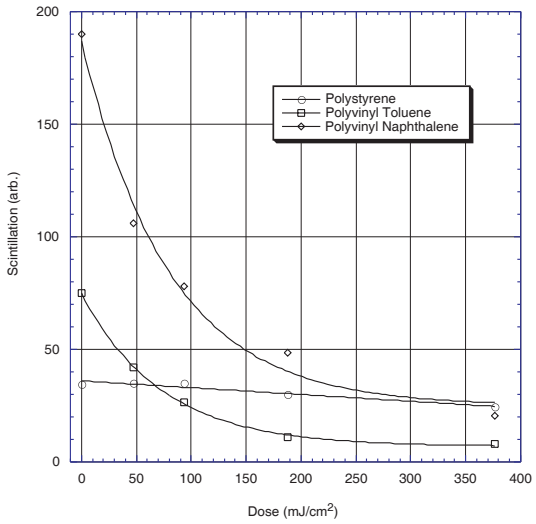

Figure 4-18: Bleaching of polymer bases with 220 nm light

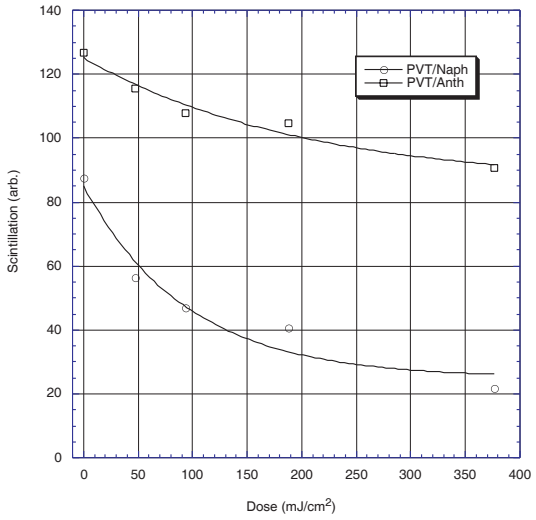

Figure 4-19: Bleaching of naphthalene and anthracene with 220 nm light

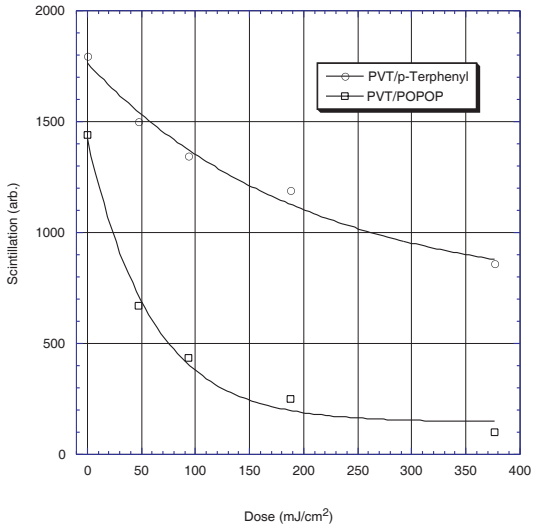

Figure 4-20: Bleaching of p-terphenyl and POPOP with 220 nm light

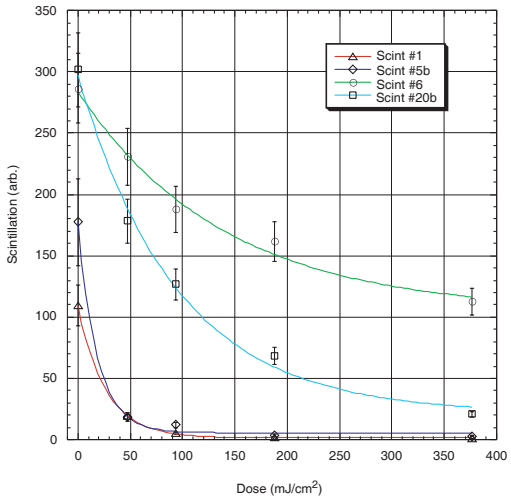

Figure 4-21: Detailed data on scintillators #1, #5, #6 and #20b, bleached at 220 nm

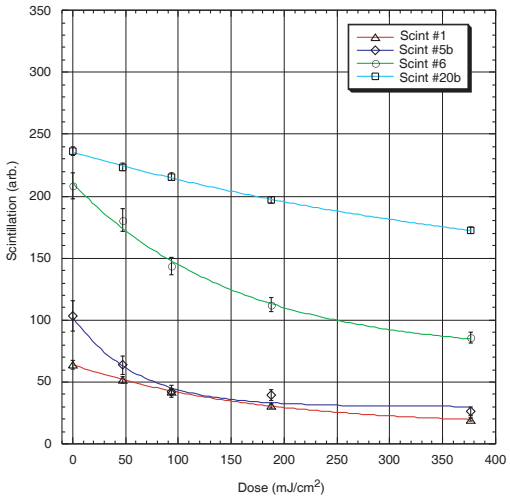

Figure 4-22: Detailed data on scintillators #1, #5, #6 and #20b, bleached at 351 nm with an ARC

Wavelength	Grating	Contrast
220	#20b (prox.)	7.5
220	#20b (cont.)	1.2
351	#1	2.2
351	#6	1.6
351	#20b	1.4

Table 4.5: Final grating contrasts

only the bleaching of a grating will be demonstrated. As mentioned in the introduction, it is not yet known what the ideal grid period should be, as this depends in a complicated fashion on the contrast, noise, and brightness of the grid as detected by the signal-locking loop [22]. It is likely, though, that periods on the order of 200 to 500 nm will be adequate, as any reasonable contrast will allow locking to less that 1% of the grid period [15]. Unfortunately, in this work grids that small were not produced due to a number of reasons, including lack of ready masks for 220 nm lithography and technical mishaps which ruined attempted interference lithography exposures at those periods. It is also not yet clear that high contrasts can be achieved at such fine periods, due to electron scattering in the scintillator. Future work will address these issues.

In this thesis, two wavelengths were used to bleach gratings: 351 and 220 nm. Scintillator #20b was the only scintillator used for the 220 nm gratings. Scintillators #1, #6, and #20b were used for 351 nm.

All gratings were bleached on top of an ARC stack, to ensure the highest possible contrast. The OAI Hybralign series 400 exposure tool was used to bleach gratings at 220 nm. As the OAI is not coherent these were not interferometric exposures, but rather were carried out with a normal photomask (5 micron period grating) in both contact and proximity modes. Gratings exposed at 351 nm were bleached with the SNL's interference lithography system. Final contrasts achieved are listed in Table 4.5. Grating images and processing data are shown in Figures 4-23 and 4-24. The procedure used to acquire and process the images is described in detail elsewhere [22].

The best contrast achieved was with the 220 nm proximity exposure. The poor contrast achieved with the 220 contact exposure is contributed to the inability of atmospheric oxygen to diffuse into the polymer during bleaching. Of the 351 nm exposures, the PMMA-based Scintilllator #1 showed the best contrast, but

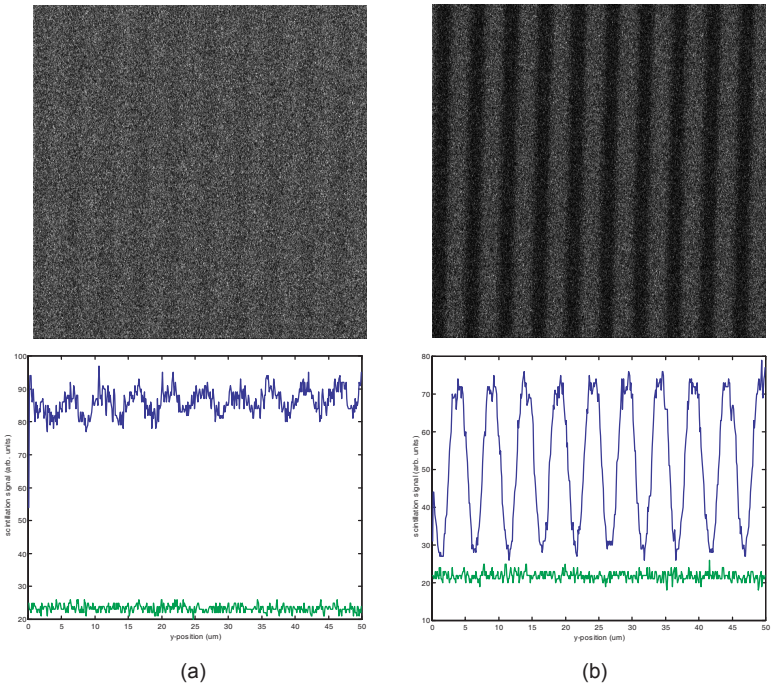

Figure 4-23: 5 micron period gratings exposed with 220 nm light in scintillator #20b: (a) contact exposure, (b) proximity exposure

by far the lowest brightness. Scintillators #6 and #20b were much brighter, but with reduced contrasts.

These contrasts are substantially different than contrasts measured with the flood-exposure technique. The reasons for this are not yet fully understood. One possible explaination is low contrast in the interference lithography exposure. Another possible explaination is the spread of the electron beam in the polymer blurs the gratings, although this seems unlikely given the energy of the electrons (5kV, which implies a Bethe range of no more than 500 nm) and the periods of the grids (1 and 5 microns).

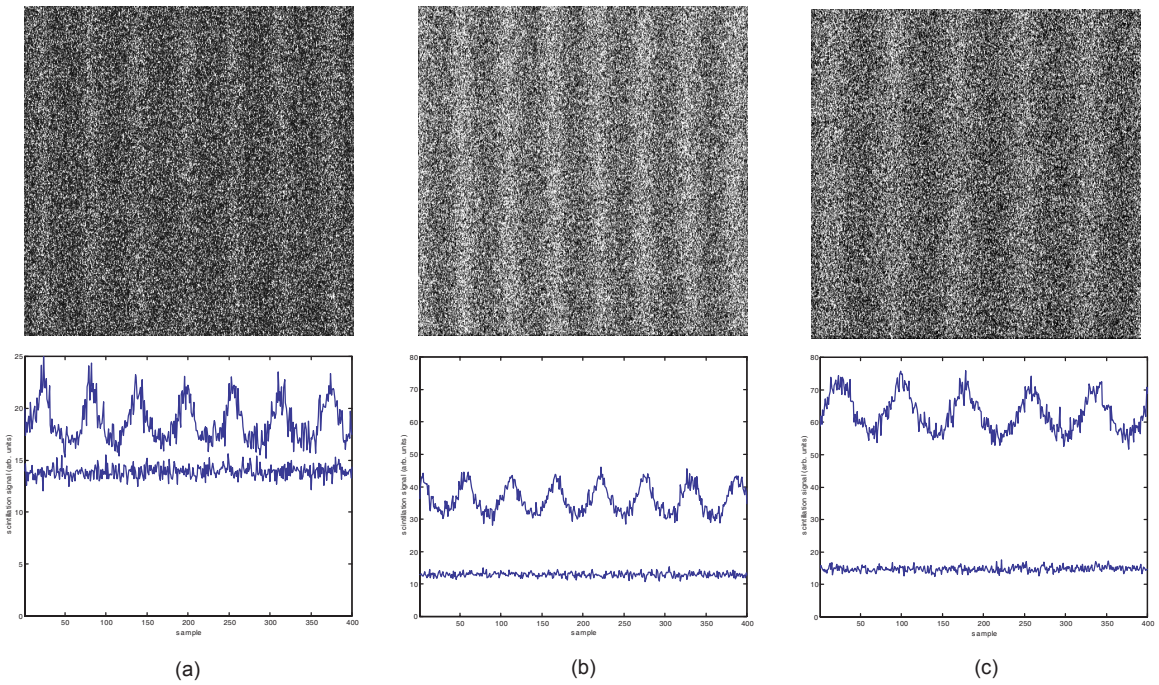

Figure 4-24: 1 micron period gratings exposed with 351 nm light: (a) scintillator #1, (b) scintillator #6, (c) scintillator #20b

Chapter 5

Summary

In the forseeable future electron-beam lithography will likely find itself unable to meet the challenge of decreasing pattern placement tolerances [1]. Spatial-phase-locked electron-beam lithography (SPLEBL) has been proposed to overcome this impending hurdle [36]. In the implementation of SPLEBL described in this thesis, a grid bleached in a scintillating polymer provides the feedback mechanism [18].

It was the intention of the work described in this thesis to formulate a general solution for the scintillating reference grid for SPLEBL. A wide variety of scintillators was explored, and those with the best contrast and brightness were investigated in detail using standardized experimental techniques. The brightest scintillator proved to be scintillator #20b which has a poly(vinyl toluene) base with p-terphenyl as the primary scintillator and POPOP as the secondary scintillator.

In addition to work on improving brightness of the scintillators, several techniques were explored to improve the contrast of the scintillators. The most important of was the the use of 220 nm light to bleach the scintillators more thoroughly. Scintillator #1, with a PMMA-base with anthracene as the primary, POPOP as the secondary, and a naphthalene additive [18], proved to have the best contrast in every technique, but had a very low brightness, and thus a noisy signal. This range of scintillators (high brightness and low contrast vs. low brightness and high contrast) may be useful as SPLEBL is further developed and it becomes more clear what parameters are most important for accurate locking to the grid.

Work on bleachable salts was carried out with the hope of developing a scheme that would improve the robustness of grid bleaching to low-contrast exposure techniques. This technique was based on the contrast-enhanced lithography scheme [19].

Fiducial gratings (one-half of a grid) were demonstrated at both 351 and 220 nm bleaching wavelengths in Scintillator #20b, as well as at 351 in Scintillators #1 and #6. Excellent contrasts, greater than 10, were achieved at 220 nm bleaching. While very close to a final mark of effectiveness for the scintillator, the true test will be the demonstration of effective pattern placement in a full-fledged SPLEBL scheme, with the scintillator fully integrated into the stack. For research purposes, a viable stack using the scintillator developed in this thesis would involve spinning scintillator on silicon, interference lithography exposures at 220 nm or lower to define the grid, then the deposition of an interlayer and spinning of the electron-beam resist. Then, dry pattern-transfer techniques would be used to bring the pattern to the substrate through the scintillator layer. A stack such as this would be appropriate for academic research aiming for a proof-of-concept of SPLEBL, but might be desirable (or even suitable) for an industrial environment. Experiments with this stack will have to wait until a 2-D SPLEBL scheme is fully operational [22].

5.1 Future Work

There are several veins to explore in future work on the scintillator. The first of these is testing additional scintillating systems. More reactive primary scintilltors such as 9-methoxy anthracene, 9,10-dimethoxy anthracene, or 9,10-bis(phenylethynyl) anthracene have been suggested to improve the bleaching contrast at 351 nm, the preferred wavelength of bleaching. Two additional schemes were suggested by the Swager group, that of a fluorophore that bleaches in the presence of phenol, using a hydroxystyrene based resist as

a polymer host (one that produces a phenol group upon ultraviolet exposure), and trying a hydroxystyrene based chemically amplified resist (which scintillate naturally).

Another important issue which was not investigated to full satisfaction in this thesis is the scintillator casting solvent and the elegant integration of the scintillator into the electron-beam resist stack. It is certainly with imagination's reach that one would be able to find an approrpate solvent, given a particular electron-beam resist. To determine if such a solvent exists more exploration would need to be carried out. It is also possible that cutting-edge research in the field of electronic polymers will soon beget a water/IPA/methanol soluble scintillating polymer, which could possibly be bleached by Rose-Bengal dye or a photoacid generator. More developments from the chemists will determine the viability of these routes.

Further investigation is neccesary into the production and resultant contrast of fine-period grids bleached at both 351 and 220 nm wavelengths (ideally, with 500 nm period or less). This issue was not fleshed out completely in this work, and still may hold some unforeseen diffculties.

Finally, as already noted, it would be neccessary to demonstrate the use of the scintillator in conjuction with SPLEBL in writing patterns with a placement accuracy better than 1 nm. This requires the completion of a full-fledged implementation of SPLEBL, work that is currently ongoing.

References

[1] Semiconductor Industry Association. International technology roadmap for semiconductors: 1999 edition. International SEMATECH, Austin, TX, 1999. Table 41b: Mask requirements – Long Term.

[2] Semiconductor Industry Association. International technology roadmap for semiconductors: 1999 edition. International SEMATECH, Austin, TX, 1999.

[3] P.W. Atkins. *Molecular Quantum Mechanics*. Oxford University Press, New York, New York, second edition, 1983.

[4] I.B. Berlman. *Handbook of Fluorescence Spectra of Aromatic Molecules*. Academic Press, New York, New York, second edition, 1971.

[5] J.B. Birks. *The Theory and Practice of Scintillation Counting*. MacMillan, Inc., New York, New York, 1964.

[6] M.J. Bowden and L.F. Thompson. Electron irradiation of poly(olefin sulfones). application to electron beam resists. *Journal of Applied Polymer Science*, 17:3211, 1973.

[7] M.J. Bowden, L.F. Thompson, and J.P. Ballantyne. Poly(butene-1 sufone) – a highly sensitive positive resist. *Journal of Vacuum Science and Technology*, 12(6):1294, 1975.

[8] H.E. Bronstein. Unpublished organic synthesis. By special request, 2000.

[9] H.E. Bronstein. Unpublished organic synthesis. By special request, 2001.

[10] ZEON Coroporation. http://www.zeon.co.jp. Furukawa Sogo Building, 2-6-1 Marunouchi, Chiyoda-ku, Tokyo, Japan, 100-8323; +81-3-3216-1772, July 2001.

[11] Bicron Corporation. http://www.bicronne.com. 6801 Cochran Road, Solon, OH, 44139; (800) 472-5656, June 2001.

[12] M. Endo, M. Sasago, Y. Hirai, K. Ogawa, and T. Ishihara. New water-soluble contrast enhancing material fo i-line lithography. *Journal of the Electrochemical Society*, 136(2):508, 1989.

[13] J. Fujita, Y. Ohnishi, Y. Ochiai, and S. Matsui. Ultrahigh resolution of calixarene negative resist in electron beam lithography. *Applied Physics Letters*, 68(9):1297, 1996.

[14] M. Furst and H. Kallmann. Enhancement of fluorescence in solutions under high-energy irradiation. *Physical Review*, 97(3):583, 1955.

[15] J. Goodberlet, J. Ferrera, and H.I. Smith. Analogue delay-locked loop for spatial-phase locking. *Electronics Letters*, 33(15):1269, 1997.

[16] J.G. Goodberlet. Unpublished data. Lab notebook, March 2000.

[17] J.G. Goodberlet. Private communication. Email communique, June 2001.

[18] J.G. Goodberlet, J. Carter, and H.I. Smith. Scintillating global-fiducial grid for electron-beam lithography. *Journal of Vacuum Science Technology B*, 16(6):3672, 1998.

[19] B.F. Griffing and P.R. West. Contrast enhanced photolithography. *IEEE Electron Device Letters*, EDL-4(1):14, 1983.

[20] L.F. Halle. A water solutble contrast enhancement layer. *Journal of Vacuum Science and Technlogy B*, 3(1):323, 1985.

[21] Hamamatsu Corporation, 360 Foothill Road, Bridgewater, NJ, 06607. *Hamamatsu Datasheet, Photomultiplier Tubes R6094-R6095*, 1996.

[22] T.J. Hastings. *Ph.D. Thesis In Progress.* PhD dissertation, MIT, Department of EECS, Nanostructures Laboratory, 2001.

[23] T.J. Hastings, F. Zhang, M.A. Finlayson, J.G. Goodberlet, and H.I. Smith. Two-dimensional spatial-phase-locked electron-beam lithography via sparse sampling. *Journal of Vacuum Science and Technology B*, 18(6):3268, 2000.

[24] G.F. Knoll. *Radiation Detection and Measurement.* John Wiley & Sons, Inc., New York, New York, third edition, 2000.

[25] D.F. Kyser. Spatial resolution limits in electron beam lithography. *Journal of Vacuum Science and Technology B*, 1(4):1391, 1983.

[26] I.N. Levine. *Quantum Chemistry.* Prentice Hall, Upper Saddle River, New Jersey, fifth edition, 2000.

[27] M.E. Walsh. Nanostructuring of magnetic thin films using interference lithography. Master of science in electrical engineering dissertation, MIT, Department of EECS, Nanostructures Laboratory, August 2000.

[28] W.M. Moreau. *Semiconductor Lithography: Principles, Practices and Materials.* Plenum Press, New York, New York, 1988.

[29] H. Namatsu, M. Nagase, K. Kurihara, K. Iwadate, T. Furuta, and K. Murase. Fabrication of sub-10-nm silicon lines with minimum fluctuation. *Journal of Vacuum Science and Technology B*, 13(4):1473, 1995.

[30] T. Perera. Antireflective coatings – an overview. Solid State Technology, Nashua, NH, July 1995.

[31] W.R. Runyan and K.E. Bean. *Semiconductor Integrated Circuit Processing Technology.* Addison-Wesley Publishing Company, Reading, MA, 1990.

[32] M.L. Schattenburg, C. Chen, P.N. Everett, J. Ferrera, P. Konkola, and Henry I. Smith. Sub-100 nm metrology using interferometrically produced fiducials. *Journal of Vacuum Science and Technology B*, 17(6):2692, 1999.

[33] M.G. Schorr and F.L Torney. Solid non-crystalline scintillation phosphors. *Physical Review*, 80(3):474, 1950.

[34] H.I. Smith. Private communication. Email communique, June 2001.

[35] H.I. Smith. *Submicron- and Nanometer-Structures Technology.* Nanostructures Press, Sudbury, MA, 2001.

[36] H.I. Smith, S.D. Hector, M.L. Schattenburg, and E.H. Anderson. A new approach to high-fidelity electron-beam lithography based on an in-situ, global fiducial grid. *Journal of Vacuum Science and Technology B*, 9:2992, 1991.

[37] R.K. Swank and W.L. Buck. The scintillation process in plastic solutions. *Physical Review*, 91:927, 1953.

[38] S.M Sze. *Physics of Semiconductor Devices.* John Wiley & Sons, Inc., New York, NY, 1981.

[39] T. Tada. Highly sensitive positive electron resists consisting of halogenated alkyl α-chloroacrylate series polymer materials. *Journal of the Electrochemical Society*, 130:912, 1983.

[40] N.J. Turro. *Modern Molecular Photochemistry*. The Benjamin/Cummings Publishing Co., Inc., Menlo Park, California, 1978.

[41] S.-I. Uchino, T. Ueno, T. Iwayanagi, h. Morishita, S. Nonogaki, S.-I. Shirai, and N. Moriuchi. Contrast enhancement materials using water soluble diazonium salts for g-line stepper. *Proceedings of the ACS Polymeric Materials Science and Engineering*, 55:604, 1986.

[42] F.C.M.J.M. van Delft and J.P. Weterings. Hydrogen silsesquioxane/novolak bilayer resist for high aspect ratio nanoscale electron-beam lithography. *Journal of Vacuum Science and Technology B*, 18(6):3419, 2000.

[43] P.R. West, G.C. Davis, and B.F. Griffing. Contrast enhanced photolithography: Application of photobleaching processes in microlithography. *Journal of Imaging Science*, 30:65, 1986.

[44] J.-S. Yang and T.M. Swager. The scintillation process in plastic solutions. *T. M. J. Am. Chem. Soc.*, 120:5321, 1998.

[45] Z. Zhu and T.M. Swager. Zhengguo polymer. Unpublished Results, June 2000.